

1 **Impacts of biogenic polyunsaturated aldehydes on metabolism and community**
2 **composition of particle-attached bacteria in coastal hypoxia**

3 Zhengchao Wu^{1,2}, Qian P. Li^{1,2,3,*}, Zaiming Ge^{1,3}, Bangqin Huang⁴, Chunming Dong⁵

4 ¹State Key Laboratory of Tropical Oceanography, South China Sea Institute of Oceanology, Chinese
5 Academy of Sciences, Guangzhou, China

6 ²Southern Marine Science and Engineering Guangdong Laboratory, Guangzhou, China

7 ³College of Marine Science, University of the Chinese Academy of Sciences, Beijing, China

8 ⁴Fujian Provincial Key Laboratory of Coastal Ecology and Environmental Studies, State Key Laboratory of
9 Marine Environmental Science, Xiamen University, Xiamen, China

10 ⁵Key Laboratory of Marine Genetic Resources, Third Institute of Oceanography, MNR, Xiamen, China

11 *Correspondence to: Qian Li (qianli@scsio.ac.cn)

12

13 **Abstract.** Eutrophication-driven coastal hypoxia is of great interest for decades, though its mechanisms
14 remain not fully understood. Here, we showed elevated concentrations of particulate and dissolved
15 polyunsaturated aldehydes (PUAs) associated with the hypoxic waters in the bottom layer of a salt-wedge
16 estuary. Bacterial respiration within the hypoxic waters was mainly contributed by particle-attached
17 bacteria (PAB) ($>0.8 \mu\text{m}$), with free-living bacteria ($0.2\text{-}0.8 \mu\text{m}$) only accounting for 25-30 % of the total
18 rate. The concentration of particle-adsorbed PUAs ($\sim 10 \mu\text{mol L}^{-1}$) in the hypoxic waters were directly
19 quantified for the first time based on large-volume-filtration and subsequent on-site PUAs derivation and
20 extraction. PUAs-amended incubation experiments for PAB ($>25 \mu\text{m}$) retrieved from the low-oxygen
21 waters were also performed to explore the impacts of PUAs on the growth and metabolism of PAB and
22 associated oxygen utilization. We found an increase in cell growth of PAB in response to low-dose PUAs (1
23 $\mu\text{mol L}^{-1}$) but an enhanced cell-specific bacterial respiration and production in response to high-dose PUAs
24 ($100 \mu\text{mol L}^{-1}$). Improved cell-specific metabolism of PAB in response to high-dose PUAs was also

25 accompanied by a shift of PAB community structure with increased dominance of genus *Alteromonas*
26 within the Gammaproteobacteria. We thus conclude that a high PUAs concentration associated with
27 aggregate particles within the bottom layer may be crucial for some species within *Alteromonas* to regulate
28 PAB community structure. The change of bacteria community could lead to an enhancement of oxygen
29 utilization during the degradation of particulate organic matters and thus likely contribute to the formation
30 of coastal hypoxia. These findings are potentially important for coastal systems with large river inputs,
31 intense phytoplankton blooms driven by eutrophication, as well as strong hypoxia developed below the
32 salt-wedge front.

33 **1. Introduction**

34 Coastal hypoxia, defined as dissolved oxygen levels $< 62.5 \mu\text{mol kg}^{-1}$, has become a worldwide problem in
35 recent decades (Diaz and Rosenberg, 2008; Helm et al., 2011). It could affect diverse life processes from
36 genes to ecosystems, resulting in the spatial and temporal change of marine food-web structures (Breitburg
37 et al., 2018). Coastal deoxygenation is also tightly coupled with other global issues, such as global warming
38 and ocean acidification (Doney et al., 2012). Formation and maintenance of eutrophication-derived hypoxia
39 in the coastal waters should reflect the interaction between physical and biogeochemical processes (Kemp
40 et al., 2009). Generally, seasonal hypoxia occurs in the coastal ocean when strong oxygen sinks are coupled
41 with restricted resupply during periods of strong density stratification. Termination of the event occurs with
42 oxygen resupply when stratification is eroded by vertical mixing (Fennel and Testa, 2019).

43 Bacterial respiration accounts for the largest portion of aquatic oxygen consumption and is thus pivotal
44 for the development of hypoxia and oxygen minimum zones (Williams and del Giorgio, 2005; Diaz and
45 Rosenberg, 2008). Generally, free-living bacteria (FLB) dominate the community respiration in many parts
46 of the ocean (Robinson and Williams, 2005; Kirchman, 2008). Compared to the FLB, the role of
47 particle-attached bacteria (PAB) on community respiration is less addressed, particularly in the coastal
48 oceans. In some coastal waters, PAB could be more abundant than the FLB with a higher metabolic activity
49 to affect the coastal carbon cycle through organic matter remineralization (Garneau et al., 2009; Lee et al.,
50 2015). An increased contribution of PAB to respiration relative to FLB can occur during the development of
51 coastal phytoplankton bloom (Huang et al., 2018). In the Columbia River estuary, the particle-attached
52 bacterial activity could be 10-100 folds higher than that of its free-living counterparts leading to its
53 dominant role in organic detritus remineralization (Crump et al., 1998). Therefore, it is crucial to assess the
54 respiration process associated with PAB and its controlling factors in these regions, to fully understand
55 oxygen utilization in the hypoxic area with an intense supply of particulate organic matters.

56 There is an increasing area of seasonal hypoxia in the nearshore bottom waters of the Pearl River
57 Estuary (PRE) and the adjacent northern South China Sea (NSCS) (Yin et al., 2004; Zhang and Li 2010; Su

58 et al., 2017). The hypoxia is generally developed at the bottom of the salt-wedge where downward mixing
59 of oxygen is restrained due to increased stratification and where there is an accumulation of
60 eutrophication-derived organic matter due to flow convergence driven by local hydrodynamics (Lu et al.,
61 2018). Besides physical and biogeochemical conditions, aerobic respiration is believed the ultimate cause
62 of hypoxia here (Su et al., 2017). Thus, microbial respiration had been strongly related to the consumption
63 of bulk dissolved organic carbon in the PRE hypoxia (He et al., 2014).

64 Phytoplankton-derived polyunsaturated aldehydes (PUAs) are known to affect marine microorganisms
65 over various trophic levels by acting as infochemicals and/or by chemical defenses (Ribalet et al., 2008;
66 Ianora and Miralto, 2010; Edwards et al., 2015; Franzè et al., 2018). PUAs are produced by stressed
67 phytoplankters during the oxidation of membrane polyunsaturated fatty acids (PUFA) by lipoxygenase
68 (Pohnert 2000) and are released from the surface of particles to the seawater by diffusion. The level of
69 PUAs in the water-column are inhomogeneous, varying from sub-nanomolar offshore to nanomolar
70 nearshore (Vidoudez et al., 2011; Wu and Li, 2016; Bartual et al., 2018), and to micromolar associated with
71 particle hotspots (Edwards et al., 2015). The strong effect of PUAs on bacterial growth, production, and
72 respiration has been well demonstrated in laboratory studies (Ribalet et al., 2008) and field studies (Balestra
73 et al., 2011; Edwards et al., 2015). A perennial bloom of PUA-producing diatoms in the PRE mouth (Wu
74 and Li, 2016) may indicate the relative importance of PUAs for microbial activity here compared to many
75 other organic compounds, such as 2-n-pentyl-4-quinolinol (Long et al., 2003) and acylated homoserine
76 lactones (Hmelo et al., 2011). A nanomolar level of PUAs recently reported in the coastal waters outside the
77 PRE was hypothesized to affect oxygen depletion by promoting microbial utilization of organic matters in
78 the bottom waters (Wu and Li, 2016). Meanwhile, the actual role of PUAs on bacterial metabolism within
79 the bottom hypoxia remains largely unexplored.

80 In this study, we investigate the particle-attached bacteria within the core of the hypoxic waters by
81 exploring the linkage between PUAs and bacterial oxygen utilization on the suspended organic particles.
82 There are three specific questions to address here: What are the relative roles of PAB and FLB on bacterial

83 respiration in the hypoxic waters? What are the actual levels of PUAs in the hypoxic waters? What are the
84 responses of PAB to PUAs in the hypoxic waters? For the first question, size-fractionated bacterial
85 respiration rates were estimated for both FLB (0.2-0.8 μm) and PAB ($>0.8 \mu\text{m}$) in the hypoxic waters. For
86 the second question, the concentrations of particulate and dissolved PUAs within the hypoxic waters were
87 measured in the field. Besides, the hotspot PUAs concentration associated with the suspended particles
88 within the hypoxic waters was directly quantified for the first time using large-volume filtration and
89 subsequent on-site derivation and extraction. For the third question, field PUAs-amended incubation
90 experiments were conducted for PAB ($>25 \mu\text{m}$) retrieved from the low-oxygen waters. We focused on
91 particles of $>25 \mu\text{m}$ to better explore the role of PUAs on PAB given the accumulations of PUAs on large
92 aggregates. The doses of PUAs treatments were selected to represent the actual levels of PUAs hotspots, to
93 assess the PAB responses (including bacterial abundance, respiration, production, and community
94 composition) to the exogenous PUAs in the hypoxic waters. By synthesizing these experimental results
95 with the change of water-column biogeochemistry, we hope to explore the underlying mechanism for
96 particle-adsorbed PUAs influencing on community structure and metabolism of PAB in the low-oxygen
97 waters, as well as to understand its contribution to coastal deoxygenation of the NSCS shelf-sea.

98

99 **2. Methods**

100 **2.1 Descriptions of field campaigns and sampling approaches**

101 Field survey cruises were conducted in the PRE and the adjacent NSCS during June 17th-28th, 2016 and
102 June 18st-July 2nd, 2019 (Figure 1). Briefly, vertical profiles of temperature, salinity, dissolved oxygen, and
103 turbidity were acquired from a Seabird 911 rosette sampling system. The oxygen sensor data were corrected
104 by field titration measurements during the cruise. Water samples at various depths were collected using 6 or
105 12 liters (12 or 24 positions) Niskin bottles attached to the Rosette sampler. Surface water samples were
106 collected at $\sim 1\text{m}$ or 5m depth, while bottom water samples were obtained at depths $\sim 4 \text{m}$ above the bottom.
107 Chlorophyll-*a* (Chl-*a*) samples were taken at all depths at all stations and nutrients were also sampled

108 except at a few discrete stations. For the 2016 cruise, samples for pPUAs were collected at all depths close
109 to station X1 (Figure 1A). During the summer of 2019, vertical profiles of particulate PUAs (pPUAs) and
110 dissolved PUAs (dPUAs) were determined at Y1 in the hypoxic zone and Y2 outside the hypoxic zone with
111 field PUAs-amended experiments conducted at Y1 (Figure 1B). For station Y1, the middle layer was
112 defined as 12 m with the bottom layer as 25 m. At this station, samples at different depths were collected
113 for determining the size-fractionated respiration rates and the whole water bacterial taxonomy.

114

115 **2.2 Determination of chlorophyll-*a*, dissolved nutrients**

116 For Chl-*a* analyses, 500 mL of water sample was gently filtered through a 0.7 μm Whatman GF/F filter.
117 The filter was then wrapped by a piece of aluminum foil and stored at $-20\text{ }^{\circ}\text{C}$ on board. Chl-*a* was extracted
118 at $4\text{ }^{\circ}\text{C}$ in the dark for 24 h using 5 mL of 90% acetone. After centrifuged at 4000 rpm for 10 min, Chl-*a*
119 was measured using a standard fluorometric method with a Turner Designs fluorometer (Parsons et al.,
120 1984). Water samples for nutrients were filtered through 0.45 μm Nucleopore filters and stored at $-20\text{ }^{\circ}\text{C}$.
121 Nutrient concentrations including nitrate plus nitrite, phosphate, and silicate were measured using a
122 segmented-flow nutrient autoanalyzer (Seal AA3, Bran-Luebbe, GmbH).

123

124 **2.3 Sampling and measurements of particulate and dissolved PUAs in one-liter seawater**

125 We used a similar protocol of Wu and Li (2016) for pPUAs and dPUAs collection, pretreatment, and
126 determination. Briefly, 2-4 liters of water sample went through a GF/C filtration with both the filter and the
127 filtrate collected separately. The filter was rinsed by the derivative solution with the suspended particle
128 samples collected in a glass vial. After adding internal standard, the samples in the vial were frozen and
129 thawed three times to mechanically break the cells for pPUAs. The filtrate from the GF/C filtration was
130 also added with internal standard and transferred to a C18 solid-phase extraction cartridge. The elute from
131 the cartridge with the derivative solution was saved in a glass vial for dPUAs. Both pPUAs and dPUAs
132 samples were frozen and stored at $-20\text{ }^{\circ}\text{C}$.

133 In the laboratory, the pPUAs sample was thawed with the organic phase extracted. After the solvent
134 was evaporated with the sample concentrated and re-dissolved in hexane, pPUAs was determined using gas
135 chromatography and mass spectrometry (Agilent Technologies Inc., USA). Standards series were prepared
136 by adding certain amounts of three major PUAs to the derivative solution and went through the same
137 pretreatment and extraction steps as samples. Derivatives of dPUAs were extracted and measured by
138 similar methods as pPUAs, except that the calibration curves of dPUAs were constructed separately. The
139 units of pPUAs and dPUAs are nmol L^{-1} (nmol PUA in one-liter seawater).

140

141 **2.4 Particle collections by large-volume filtrations in hypoxia waters.**

142 Large volumes (~300 L) of the middle (12 m) and the bottom (25 m) waters within the hypoxia zone were
143 collected by Niskin bottles at station Y1. For each layer, the water sample was quickly filtered through a
144 sterile fabric screen (25 μm filter) on a disk filter equipped with a peristaltic pump to qualitatively obtain
145 particles of $>25 \mu\text{m}$. Larger zooplankters were picked off immediately. The particle samples were gently
146 back-flushed three times off the fabric screen using particle-free seawater (obtained using a 0.2 μm
147 filtration of the same local seawater) into a sterile 50-mL sampling tube.

148 The volume of total particles from large-volume-filtration was measured as follows: The collected
149 particle in the 50 mL tube was centrifuged for one minute at a speed of 3000 revolutions per minute (r.p.m)
150 with the supernatant saved (Hmelo et al., 2011). The particle sample was resuspended as slurry by gently
151 shaking and transferred into a sterile 5 mL graduated centrifuge tube. The sample was centrifuged again by
152 the same centrifuging speed with the final volume of the total particles recorded. The unit for the total
153 particle volume is mL.

154 All the particles were transferred back to the sterile 50 mL centrifuge tube (so as all the supernatants)
155 with 0.2- μm -filtered seawater, which was used for subsequent measurements of particle-adsorbed PUAs as
156 well as for PUAs-amended incubation experiments of particle-attached bacteria.

157

158 **2.5 Measurements of particle-adsorbed PUAs**

159 After gently shaking, 3 mL of sample in the 50 mL sampling tube (see section 2.4) was used for the
160 analyses of particle-adsorbed PUAs concentration (two replicates) according to the procedure shown in
161 Figure 2 (modified from the protocols of Edwards et al. 2015 and Wu and Li 2016). The sample (3 mL) was
162 transferred to 50 mL centrifuge tubes for PUAs derivatization on board. An internal standard of
163 benzaldehyde was added to obtain a final concentration of 10 μM . The aldehydes in the samples were
164 derivatized by the addition of O-(2,3,4,5,6-pentafluorobenzyl) hydroxylamine hydrochloride solution in
165 deionized water ($\text{pH}=7.5$). The reaction was performed at room temperature for 15 min (shaking slightly
166 for mix every 5 min). Then 2 mL sulfuric acid (0.1%) solution was added to a final concentration of 0.01%
167 acid (pH of 2-3) to avoid new PUAs induced by enzymatic cascade reactions. The derivate samples were
168 subsequently sonicated for 3 min before the addition of 20 mL hexane, and the upper organic phase of the
169 extraction was transferred to a clean tube and stored at $-20\text{ }^{\circ}\text{C}$.

170 Upon returning to the laboratory, the adsorbed PUAs on these particles (undisrupted PUAs) were
171 determined with the same analytical methods as those for the disrupted pPUAs (freeze-thaw methods to
172 include the portion of PUAs eventually produced as cells die, Wu and Li 2016) except for the freeze-thaw
173 step. A separate calibration curve was made for the undisrupted PUAs derivates. A standard series of
174 heptadienal, octadienal, and decadienal (0, 0.1, 0.5, 1.0, 2.5, 5.0, 10.0, 25.0 nmol L^{-1}) was prepared before
175 each analysis by diluting a relevant amount of the PUA stock solution (methanolic solution) with deionized
176 water. These standard solutions were processed through all the same experimental steps as those mentioned
177 above for derivation, extraction, and measurement of the undisrupted PUAs sample. The unit for the
178 undisrupted PUAs is nmol L^{-1} . The total amount of the undisrupted PUAs in the 50 mL sampling tube was
179 the product of the measured concentration and the total volume of the sample.

180 The hotspot PUAs concentration associated with the aggregate particles is defined as the PUAs
181 concentration in the volume of the water parcel displaced by these particles. Therefore, the final
182 concentration of particle-adsorbed PUAs in the water column, defined as PUAs [$\mu\text{mol L}^{-1}$], should be equal

183 to the moles of particle-adsorbed PUAs (nmol, the undisrupted PUAs) divided by the volume of particles
184 (mL).

185

186 **2.6 Incubation of particle-attached bacteria with PUAs treatments.**

187 The impact of PUAs on microbial growth and metabolisms in the hypoxia zone was assessed by field
188 incubation of particle-attached bacteria on particles of > 25 μm collected from large-volume filtration with
189 direct additions of low or high doses of PUAs (1 or 100 $\mu\text{mol L}^{-1}$) on June, 29th, 2019 (Figure 2).

190 A sample volume of ~32 mL in the centrifuge tube (section 2.4) was transferred to a sterile Nalgene
191 bottle before being diluted by particle-free seawater to a final volume of 4 L. About 3.2 L of the sample
192 solution was transferred into four sterile 1-L Nalgene bottles (each with 800 mL). One 1-L bottle was used
193 for determining the initial conditions: after gentle shaking, the solution was transferred into six biological
194 oxygen demand (BOD) bottles with three for initial oxygen concentration (fixed immediately by Winkler
195 reagents) and the other three for initial bacterial abundance, production, and community structure. The
196 other three 1-L bottles were used for three different treatments (each with two replicates in two 0.5-L
197 bottles): the first one served as the control with the addition of 200 μL methanol, the second one with 200
198 μL low-dose PUAs solution, and the third one with 200 μL high-dose PUAs solution (Table 1). The
199 solution in each of the three treatments (0.5L bottles) was transferred to six parallel replicates by 60-mL
200 BOD bottles. These BOD bottles were incubated at *in situ* temperature in the dark for 12 hours. At the end
201 of each incubation experiment, three of the six BOD bottles were used for determining the final oxygen
202 concentrations with the other three for the final bacterial abundance, production, and community structure.

203 To test the possibility of PUAs as carbon sources for bacterial utilization, a minimal medium was
204 prepared with only sterile artificial seawater but not any organic carbons (Dyksterhouse et al., 1995). A
205 volume of 375 μL sample (from the above 4 L sample solution) was inoculated in the minimal medium
206 amended with heptadienal in a final concentration of about 200 $\mu\text{mol L}^{-1}$. This PUA level was close to the
207 hotspot PUAs of 240 $\mu\text{mol L}^{-1}$ found in the suspended particles of a station near the PRE. It was also

208 comparable to the hotspot PUAs of $25.7 \mu\text{mol L}^{-1}$ in the temperate west North Atlantic (Edwards et al.,
209 2015). For comparisons, the same amount of sample was also inoculated in the minimal medium (75 mL)
210 amended with an alkane mixture (ALK, n-pentadecane and n-heptadecane) at a final concentration of 0.25
211 g L^{-1} , or with a mixture of polycyclic aromatic hydrocarbons (PAH, naphthalene and phenanthrene) at a
212 final concentration of 200 ppm. These experiments were performed in dark at room temperature for over 30
213 days. Significant turbidity changes in the cell culture bottle over incubation time will be observed if there is
214 a carbon source for bacterial growth.

215

216 **2.7 Measurements of bacteria-related parameters**

217 **(1) Bacterial abundance**

218 At the end of the 12-h incubation period, a 2 mL sample from each BOD bottle was preserved in 0.5%
219 glutaraldehyde. The fixation lasted for half of an hour at room temperature before being frozen in liquid N_2
220 and stored in a $-80 \text{ }^\circ\text{C}$ freezer. In the laboratory, the samples were performed through a previously
221 published procedure for detaching particle-attached bacteria (Lunau et al., 2005), which had been proved
222 effective for samples with high particle concentrations. To break up particles and attached bacteria, 0.2 mL
223 pure methanol was added to the 2 mL sample and vortexed. The sample was then incubated in an ultrasonic
224 bath (35 kHz, 2 x 320W per period) at $35 \text{ }^\circ\text{C}$ for 15 min. Subsequently, the tube sample was filtered with a
225 $50 \mu\text{m}$ -filter to remove large detrital particles. The filtrate samples for surface-associated bacteria cells
226 were diluted by 5-10 folds using TE buffer solution and stained with 0.01% SYBR Green I in the dark at
227 room temperature for 40 min. With the addition of $1\text{-}\mu\text{m}$ beads, bacterial abundance (BA) of the samples
228 was counted by a flow cytometer (Beckman Coulter CytoFlex S) with bacteria detected on a plot of green
229 fluorescence versus side scatter (Marie et al., 1997). The precision of the method estimated by the
230 coefficient of variation (CV%) was generally less than 5%.

231 For bulk-water bacteria abundance (including both FLB and PAB), 1.8 mL of seawater sample was
232 collected after a $20\text{-}\mu\text{m}$ prefiltration. The sample was transferred to a 2 mL centrifuge tube and fixed by

233 adding 20 μL of 20% paraformaldehyde before storage in a $-80\text{ }^{\circ}\text{C}$ freezer. In the laboratory, 300 μL of the
234 sample after thawing was used for staining with SYBR Green and analyzed using the same flow cytometry
235 method as above (Marie, et al, 1997).

236

237 **(2) Bacterial respiration**

238 For BOD samples, bacterial respiration (BR) was calculated based on the oxygen decline during the 12-h
239 incubation and was converted to carbon units with the respiratory quotient assumed equal to 1 (Hopkinson,
240 1985). Dissolved oxygen was determined by a high-precision Winkler titration apparatus (Metrohm-848,
241 Switzerland) based on the classic method (Oudot et al., 1988). We should mention that BR could be
242 overestimated if phytoplankton and microzooplankton were present in the particle aggregates of $> 25\text{ }\mu\text{m}$.
243 However, this effect could be relatively small because the raw seawater in the hypoxic zone had very low
244 chlorophyll-*a* and because there was virtually not much microzooplankton in the sample (confirmed by
245 FlowCAM).

246 Method for the estimation of the bulk water bacterial respiration at stations X1, X2, and X3 can be
247 found in Xu et al (2018). For the bulk water at station Y1, the size-fractionated respiration rates, including
248 free-living bacteria of $0.2\text{-}0.8\text{ }\mu\text{m}$ and particle-associated community of $>0.8\text{ }\mu\text{m}$ (we assumed that they
249 were mostly PAB given the low phytoplankton chlorophyll-*a* of the sample and the absence of zooplankton
250 during the filtration), were estimated based on the method of García-Martín et al (2019). Four 100 mL
251 polypropylene bottles were filled with seawater. One bottle was immediately fixed by formaldehyde. After
252 15 min, the sample in each bottle was incubated in the dark at the *in situ* temperature after the addition of
253 the Iodo-Nitro-Tetrazolium (INT) salt at a final concentration of 0.8 mmol L^{-1} . The incubation reaction
254 lasted for 1.5 h before being stopped by formaldehyde. After 15 min, all the samples were sequentially
255 filtered through 0.8 and $0.2\text{ }\mu\text{m}$ pore size polycarbonate filters and stored frozen until further measurements
256 by spectrophotometry.

257

258 **(3) Bacterial production**

259 Bacterial production (BP) was determined using a modified protocol of the ^3H -leucine incorporation
260 method (Kirchman, 1993). Four 1.8-mL aliquots of the sample were collected by pipet from each BOD
261 incubation and added to 2-mL sterile microcentrifuge tubes, which were incubated with ^3H -leucine (in a
262 final concentration of $4.65 \mu\text{mol Leu L}^{-1}$, Perkin Elmer, USA). One tube served as the control was fixed by
263 adding 100% trichloroacetic acid (TCA) immediately (in a final concentration of 5%). The other three were
264 terminated with TCA at the end of the 2-h dark incubation. Samples were filtered onto 0.2- μm
265 polycarbonate filters and then rinsed twice with 5% TCA and three times with 80% ethanol (Huang et al.,
266 2018) before being stored at $-80 \text{ }^\circ\text{C}$. In the laboratory, the filters were transferred to scintillation vials with
267 5 mL of Ultima Gold scintillation cocktail. The incorporated ^3H was determined using a Tri-Carb 2800TR
268 liquid scintillation counter. Bacterial production was calculated with the previous published
269 leucine-to-carbon empirical conversion factors of $0.37 \text{ kg C mol leucine}^{-1}$ in the study area (Wang et al.,
270 2014). Bacterial carbon demand (BCD) was calculated as the sum of BP and BR. Bacterial growth
271 efficiency (BGE) was equated to BP/BCD .

272

273 **(4) Bacterial community structure**

274 At the end of incubation, the DNA sample was obtained by filtering 30 mL of each BOD water via a
275 0.22- μm Millipore filter, which was preserved in a cryovial with the DNA protector buffer and stored at
276 $-80 \text{ }^\circ\text{C}$. DNA was extracted using the DNeasy PowerWater Kit with genomic amplification by Polymerase
277 Chain Reaction (PCR). The V3 and V4 fragments of bacterial 16S rRNA were amplified at $94 \text{ }^\circ\text{C}$ for 2 min
278 and followed by 27 cycles of amplification ($94 \text{ }^\circ\text{C}$ for 30 s, $55 \text{ }^\circ\text{C}$ for 30 s, and $72 \text{ }^\circ\text{C}$ for 60 s) before a
279 final step of $72 \text{ }^\circ\text{C}$ for 10 min. Primers for amplification included 341F (CCTACGGGNGGCWGCAG) and
280 805R (GACTACHVGGGTATCTAATCC). Reactions were performed in a 10- μL mixture containing 1 μL
281 Toptaq Buffer, 0.8 μL dNTPs, 10 μM primers, 0.2 μL Taq DNA polymerase, and 1 μL Template DNA.
282 Three parallel amplification products for each sample were purified by an equal volume of AMPure XP

283 magnetic beads. Sample libraries were pooled in equimolar and paired-end sequenced (2×250 bp) on an
284 Illumina MiSeq platform.

285 High-quality sequencing data was obtained by filtering on the original off-line data. Briefly, the raw
286 data was pre-processed using TrimGalore to remove reads with qualities of less than 20 and FLASH2 to
287 merge paired-end reads. Besides, the data were also processed using Usearch to remove reads with a total
288 base error rate of greater than 2 and short reads with a length of less than 100 bp and using Mothur to
289 remove reads containing more than 6 bp of N bases. We further used UPARSE to remove the singleton
290 sequence to reduce the redundant calculation during the data processing. Sequences with similarity greater
291 than 97% were clustered into the same operational taxonomic units (OTUs). R software was used for
292 community composition analysis.

293 DNA samples for the bulk bacteria (>0.2 µm) and PAB on particles of > 25 µm at station Y1 were also
294 collected for bacterial community analysis using the same method described above. Methods for the bulk
295 water bacterial community analyses at stations X1, X2, and X3 during the 2016 cruise can be found in the
296 published paper of Xu et al. (2018).

297

298 **2.8 Statistical Analysis**

299 All statistical analyses were performed using the statistical software SPSS (Version 13.0, SPSS Inc.,
300 Chicago, IL, USA). A student's t-test with a 2-tailed hypothesis was used when comparing PUAs-amended
301 treatments with the control or comparing stations inside and outside the hypoxic zone, with the null
302 hypothesis being rejected if the probability (p) is less than 0.05. We consider p of <0.05 as significant and p
303 of <0.01 as strong significant. Ocean Data View with the extrapolation model "DIVA Gridding" method
304 was used to contour the spatial distributions of physical and biogeochemical parameters.

305

306 **3. Results**

307 **3.1 Characteristics of hydrography, biogeochemistry, and bulk bacteria community in the hypoxic**

308 **zone**

309 During our study periods, there was a large body of low oxygen bottom water with the strongest hypoxia (<
310 $62.5 \mu\text{mol kg}^{-1}$) on the western shelf of the PRE (Figure 1), which was relatively similar among different
311 summers of 2016 and 2019 (Figure 1). For vertical distribution, a strong salt-wedge structure was found
312 over the inner shelf (Figures 3A, 3D) with freshwater on the shore side due to intense river discharge.
313 Bottom waters with oxygen deficiency (< $93.5 \mu\text{mol kg}^{-1}$) occurred below the lower boundary of the
314 salt-wedge and expanded ~60 km offshore (Figure 3E). In contrast, a surface high Chl-*a* patch ($6.3 \mu\text{g L}^{-1}$)
315 showed up near the upper boundary of the front, where there was enhanced water-column stability, low
316 turbidity, and high nutrients (Figures 3B, 3C). Therefore, there was a spatial mismatch between the
317 subsurface hypoxic zone (Figure 3E) and the surface chlorophyll-bloom (Figure 3F) during the
318 estuary-to-shelf transect, as both the surface Chl-*a* and oxygen right above the hypoxic zones at the bottom
319 boundary of the salt-wedge were not themselves maxima.

320 There were much higher rates of respiration (BR) ($t=7.8$, $n=9$, $p<0.01$) and production (BP) ($t=13.0$,
321 $n=9$, $p<0.01$) for the bulk bacterial community (including FLB and PAB) in the bottom waters of X1 within
322 the hypoxic core than those of X2 and X3 outside the hypoxic zone during June 2016 (Figure 4, modified
323 from data of Xu et al., 2018). The size-fractionated respiration rates were quantified at station Y1 during the
324 2019 cruise (Figure S1) to distinguish the different roles of FLB and PAB on bacterial respiration in the
325 hypoxic waters. Our results suggested that bacterial respiration within the hypoxic waters was largely
326 contributed by PAB ($>0.8 \mu\text{m}$), which was about 2.3-3 folds of that by FLB ($0.2-0.8 \mu\text{m}$).

327 The bulk bacterial composition of the bottom water of X1 during the 2016 cruise with 78% of
328 α -Proteobacteria (α -Pro), 15% of γ -Proteobacteria (γ -Pro), and 6% of Bacteroidetes was significantly
329 different from those of X2 and X3 (91% α -Pro, 5% γ -Pro, and 2% Bacteroidetes), although their bacterial
330 abundances were about the same (Figure 4). Compared to that of the 2016 cruise, there was a different
331 taxonomic composition of the bulk bacterial community in the hypoxic waters of the 2019 cruise with on
332 average 33% of α -Pro, 25% of γ -Pro, and 14% of Bacteroidetes. Furthermore, there was a substantially

333 different taxonomic composition for PAB (>25 μm) with on average 66% of γ -Pro, 22% of α -Pro, and 4%
334 of Bacteroidetes (Figure S2A). In particular, there was an increase of γ -Pro, but a decrease of α -Pro and
335 Bacteroidetes, in the PAB (>25 μm) relative to the bulk bacterial community. On the genus level, the PAB
336 (>25 μm) was largely dominated by the *Alteromonas* group in both the middle and bottom waters (Figure
337 S2B).

338

339 **3.2 PUAs concentrations in the hypoxic zone**

340 Generally, there were significantly higher pPUAs of 0.18 nmol L^{-1} ($t=3.20$, $n=10$, $p<0.01$) and dPUAs of
341 0.12 nmol L^{-1} ($t=7.61$, $n=8$, $p<0.01$) in the hypoxic waters than in the nearby bottom waters without
342 hypoxia (0.02 nmol L^{-1} and 0.01 nmol L^{-1}). Vertical distributions of pPUAs and dPUAs in the bulk seawater
343 were showed for two stations (Y1 and Y2) inside and outside the hypoxic zone (Figure 1). Nanomolar
344 levels of pPUAs and dPUAs were found in the water column in both stations (Figures 5E, 5F). There were
345 high pPUAs and dPUAs in the bottom hypoxic waters of station Y1 (Figure 5E, 5F) together with locally
346 elevated turbidity (Figure 3B) when compared to the bottom waters outside, which likely a result of particle
347 resuspension. For station Y2 outside the hypoxia, we found negligible pPUAs and dPUAs at depths below
348 the mixed layer (Figure 5E, 5F), which could be due to PUAs dilution by the intruded subsurface seawater.

349 Particle-adsorbed PUAs in the low-oxygen waters were quantified for the first time with the direct
350 particle volume estimated by large-volume-filtration (see the method section), which would reduce the
351 uncertainty associated with particle volume calculated by empirical equations derived for marine-snow
352 particles (Edward et al., 2015). We found high levels of particle-adsorbed PUAs ($\sim 10 \mu\text{mol L}^{-1}$) in these
353 waters (Figure 6), which were orders of magnitude higher than the bulk water pPUAs or dPUAs
354 concentrations ($<0.3 \text{ nmol L}^{-1}$, Figure 5E, 5F). Particle-adsorbed PUAs of the low-oxygen waters mainly
355 consisted of heptadienal (C7_PUA) and octadienal (C8_PUA).

356

357 **3.3 Particle-attached bacterial growth and metabolism in the hypoxic zone**

358 Incubation of the PAB acquired from the low-oxygen waters with direct additions of different doses of
359 exogenous PUAs over 12 hours was carried out to examine the change of bacterial growth and metabolism
360 activities in response to PUA-enrichments. At the end of the incubation experiments, BA was not different
361 from the control for the PH treatment (Figure 7A). However, for the PL treatment, there were substantial
362 increases of BA in both the middle and the bottom waters compared to the initial conditions (Figure 7A). In
363 particular, BA of $\sim 3.2 \pm 0.04 \times 10^9$ cells L⁻¹ in the bottom water for the PL treatment was significantly
364 higher ($t=12.26$, $n=12$, $p<0.01$) than the control of $2.5 \pm 0.07 \times 10^9$ cells L⁻¹.

365 BR was significantly promoted by the low-dose PUAs with a 21.6% increase in the middle layer
366 ($t=11.91$, $n=8$, $p<0.01$) and a 25.8% increase in the bottom layer ($t=11.50$, $n=8$, $p<0.01$) compared to the
367 controls. Stimulating effect of high-dose PUAs on BR was even stronger with 47.0% increase in the middle
368 layer ($t=30.56$, $n=8$, $p<0.01$) and 39.8% increase in the bottom layer ($t=9.40$, $n=8$, $p<0.01$) (Figure 7B).
369 Meanwhile, the cell-specific BR was significantly improved for both layers with high-dose of PUAs
370 ($t=15.13$, $n=8$, $p<0.01$ and $t=4.77$, $n=8$, $p<0.01$), but not with low-dose of PUAs (Figure 7C) due to
371 increase of BA (Figure 7A). BGE was generally very low (<1.5%) during all the experiments (Figure 7D)
372 due to substantially high rates of BR (Figure 7B) than BP (Figure 7E). Also, there was no significant
373 difference in BGE between controls and PUAs treatments for both layers (Figure 7D).

374 For the bottom layer, BP was $12.6 \pm 0.8 \mu\text{g C L}^{-1} \text{ d}^{-1}$ for low-dose PUAs and $16.4 \pm 0.6 \mu\text{g C L}^{-1} \text{ d}^{-1}$
375 for high-dose PUAs, which were both significantly ($t=2.98$, $n=8$, $p<0.05$ and $t=10.41$, $n=8$, $p<0.01$) higher
376 than the control of $10.6 \pm 0.6 \mu\text{g C L}^{-1} \text{ d}^{-1}$. Meanwhile, BP in the middle layer was significantly higher
377 ($t=2.52$, $n=8$, $p<0.05$) than the control for high-dose PUAs ($13.4 \pm 0.9 \mu\text{g C L}^{-1} \text{ d}^{-1}$) but not for low-dose
378 PUAs ($12.6 \pm 0.9 \mu\text{g C L}^{-1} \text{ d}^{-1}$) (Figure 7E). The cell-specific BP (sBP, 7.9 ± 0.5 and $6.9 \pm 0.2 \text{ fg C cell}^{-1} \text{ d}^{-1}$)
379 for high-dose PUAs were significantly ($t=2.62$, $n=8$, $p<0.05$ and $t=11.26$, $n=8$, $p<0.01$) higher than the
380 control in both layers (Figure 7F). Meanwhile, for low-dose PUAs, the sBP in both layers were not
381 significantly different from the controls.

382

383 **3.4 Particle-attached bacterial community change during incubations**

384 Generally, γ -Pro dominated (>68%) the bacterial community at the class level for all experiments, followed
385 by the second largest bacterial group of α -Pro. There was a significant increase of γ -Pro by high-dose PUAs
386 with increments of 17.2% ($t=9.25$, $n=8$, $p<0.01$) and 19.5% ($t=6.32$, $n=8$, $p<0.01$) for the middle and the
387 bottom layers, respectively (Figure 8A). However, there was no substantial change of bacterial community
388 composition by low-dose PUAs for both layers (Figure 8A).

389 On the genus level, there was also a large difference in the responses of various bacterial subgroups to
390 the exposure of PUAs (Figure 8B). The main contributing genus for the promotion effect by high-dose
391 PUAs was the group of *Alteromonas* spp., which showed a large increase in abundance by 73.9% and
392 69.7% in the middle and the bottom layers. For low-dose PUAs, the promotion effect of PUAs on
393 *Alteromonas* spp. was still found although with a much lower intensity (5.4% in the middle and 19.4% in
394 the bottom). The promotion effect of γ -Pro by high-dose PUAs was also contributed by bacteria *Halomonas*
395 spp. (percentage increase from 1.7% to 7.4%). Meanwhile, some bacterial genus, such as *Marinobacter* and
396 *Methylophaga* from γ -Pro, or *Nautella* and *Sulfitobacter* from α -Pro, showed decreased percentages by
397 high-dose PUAs (Figure 8B).

398

399 **3.5 Carbon source preclusion experiments for PUAs**

400 After one month of incubation, PAB inoculated from the low-oxygen waters showed dramatic responses to
401 both PAH and ALK (Figure 9). In particular, the mediums of PAH addition became turbid brown (bottles on
402 the left) with the medium of ALK addition turning into milky white (bottles in the middle) (Figures 9B and
403 9D). For comparison, they were both clear and transparent at the beginning of the experiments (Figures 9A
404 and 9C). These results should reflect the growth of bacteria in these bottles with the enrichments of organic
405 carbons. Meanwhile, the minimal medium with the addition of heptadienal (C7_PUA) remained clear and
406 transparent as it was originally, which would indicate that PAB did not grow in the treatment of C7_PUA.

407

408 **4. Discussion**

409 Hypoxia occurs if the rate of oxygen consumption exceeds that of oxygen replenishment by diffusion,
410 mixing, and advection (Rabouille et al., 2008). The spatial mismatch between the surface chlorophyll-*a*
411 maxima and the subsurface hypoxia during our estuary-to-shelf transect should indicate that the
412 low-oxygen feature may not be directly connected to particle export by the surface phytoplankton bloom.
413 This outcome can be a combined result of riverine nutrient input in the surface, water-column stability
414 driven by wind and buoyancy forcing, and flow convergence for an accumulation of organic matters in the
415 bottom (Lu et al., 2018).

416 Elevated concentrations of pPUAs and dPUAs near the bottom boundary of the salt-wedge should
417 reflect a sediment source of PUAs, as the surface phytoplankton above them was very low. PUA-precursors
418 such as PUFA could be accumulated as detritus in the surface sediment near the PRE mouth during the
419 spring blooms (Hu et al., 2006). Strong convergence at the bottom of the salt-wedge could be driven by
420 shear vorticity and topography (Lu et al., 2018). This would allow for the resuspension of small detrital
421 particles. Improved PUAs production by oxidation of the resuspended PUFA could occur below the
422 salt-wedge as a result of enhanced lipoxygenase activity (in the resuspended organic detritus) in response to
423 salinity increase by the intruded bottom seawater (Galeron et al., 2018).

424 Direct measurement of the adsorbed PUAs concentration associated with the suspended particles
425 of >25 μm by the method of combined large-volume filtration and on-site derivation and extraction yield a
426 high level of $\sim 10 \mu\text{mol L}^{-1}$ within the hypoxic zone. This value is comparable to those previously reported
427 in sinking particles (>50 μm) of the open ocean using particle-volume calculated from diatom-derived
428 marine snow particles (Edward et al., 2015). Note that there was also a higher level of $240 \mu\text{mol L}^{-1}$ found
429 in another station outside the PRE. A micromolar level of particle-adsorbed PUAs could act as a hotspot for
430 bacteria likely exerting important impacts as signaling molecules on microbial utilization of particulate
431 organic matters and subsequent oxygen consumption.

432 The hypoxic waters below the salt-wedge have high turbidity probably due to particle resuspension.

433 High particle concentration here may indicate the important role of PAB, which could be more abundant
434 than FLB in the turbid waters near the mouth of the PRE (Ge et al., 2020), similar to those found in the
435 Columbia River estuary (Crump et al., 1998). Also, anaerobic bacteria and taxa preferring low-oxygen
436 conditions were found more enriched in the particle-attached communities than their free-living
437 counterparts in the PRE (Zhang et al., 2016). Our field measurements suggested that bacterial respiration
438 within the hypoxic waters was largely contributed by PAB ($>0.8 \mu\text{m}$) with FLB ($0.2\text{-}0.8 \mu\text{m}$) playing a
439 relatively small role. Therefore, it is crucial to address the linkage between the high-density PAB and the
440 high level of particle-adsorbed PUAs associated with the suspended particles in the low-oxygen waters.

441 Interestingly, our PUA-amended experiments for PAB ($>25 \mu\text{m}$) retrieved from the low-oxygen waters
442 revealed distinct responses of PAB to different doses of PUAs treatments with an increase in cell growth in
443 response to low-dose PUAs ($1 \mu\text{mol L}^{-1}$) but an elevated cell-specific metabolic activity including bacterial
444 respiration and production in response to high-dose PUAs ($100 \mu\text{mol L}^{-1}$). An increase in cell density of
445 PAB by low-dose PUAs could likely reflect the stimulating effect of PUAs on PAB growth. This finding
446 was consistent with the previous report of a PUAs level of $0\text{-}10 \mu\text{mol L}^{-1}$ stimulating respiration and cell
447 growth of PAB in sinking particles of the open ocean (Edwards et al., 2015). The negligible effect of
448 low-dose PUAs on bacterial community structure in our experiments was also in good agreement with
449 those found for PAB from sinking particles (Edwards et al., 2015). However, we do not see the inhibitory
450 effect of $100 \mu\text{mol L}^{-1}$ PUAs on PAB respiration and production previously found in the open ocean
451 (Edward et al., 2015). Instead, the stimulating effect for high-dose PUAs on bacterial respiration and
452 production was even stronger with $\sim 50\%$ increments. The bioactivity of PUAs on bacterial strains could
453 likely arise from its specific arrangement of two double bonds and carbonyl chain (Ribalet et al., 2008).
454 Our findings support the important role of PUAs in enhancing bacterial oxygen utilization in low-oxygen
455 waters.

456 It should be mentioned that it remains controversial the effect of background nanomolar PUAs on
457 free-living bacteria, which is not our focus in this study. Previous studies suggested that 7.5 nmol L^{-1} PUAs

458 would have a different effect on the metabolic activities of distinct bacterial groups in the NW
459 Mediterranean Sea, although bulk bacterial abundance remained unchanged (Balestra et al., 2011). In
460 particular, the metabolic activity of γ -Pro was least affected by nanomolar PUAs, although those of
461 Bacteroidetes and Rhodobacteraceae were markedly depressed (Balestra et al., 2011). Meanwhile, the daily
462 addition of 1 nmol L⁻¹ PUAs was found to not affect the bacterial abundance and community composition
463 during a mesocosm experiment in the Bothnian Sea (Paul et al., 2012).

464 It is important to verify that the PUAs are not an organic carbon source but a stimulator for PAB
465 growth and metabolism. This was supported by the fact that the inoculated PAB could not grow in the
466 medium with 200 μ mol L⁻¹ of PUAs although they grew pretty well in the mediums with a similar amount
467 of ALK or PAH. Our results support the previous findings that the density of *Alteromonas hispanica* was
468 not significantly affected by 100 μ mol L⁻¹ of PUAs in the minimal medium (without any organic carbons)
469 during laboratory experiments (Figure 9E), where PUAs were considered to act as cofactors for bacterial
470 growth (Ribalet et al., 2008).

471 Improved cell-specific metabolism of PAB in response to high-dose PUAs was accompanied by a
472 significant shift of bacterial community structure. The group of PAB with the greatest positive responses to
473 exogenous PUAs was genus *Alteromonas* within the γ -Pro, which is well-known to have a particle-attached
474 lifestyle with rapid growth response to organic matters (Ivars-Martinez et al., 2008). This result is
475 contradicted by the previous finding of a reduced percentage of the γ -Pro class by high-dose PUAs in the
476 PAB of open ocean sinking particles (Edward et al., 2015). Meanwhile, previous studies suggested that
477 different genus groups within the γ -Pro may respond distinctly to PUAs (Ribalet et al., 2008). Our result
478 was well consistent with the previous finding of the significant promotion effect of 13 or 106 μ mol L⁻¹
479 PUAs on *Alteromonas hispanica* from the pure culture experiment (Ribalet et al., 2008). An increase of
480 PUAs could thus confer some of the γ -Pro (mainly special species within the genus *Alteromonas*, such as *A.*
481 *hispanica*, Figure S2B) a competitive advantage over other bacteria, leading to their population dominance
482 on particles in the low-oxygen waters. These results provide evidences for a previous hypothesis that PUAs

483 could shape the bacterioplankton community composition by driving the metabolic activity of bacteria with
484 neutral, positive, or negative responses (Balestra et al., 2011).

485 The taxonomic composition of PAB (>25 μm) was substantially different from that of the bulk
486 bacteria community in the hypoxic zone (with a large increase of γ -Pro associated with particles, Figure
487 S2A). This result supports the previous report of γ -Pro being the most dominant clades attached to sinking
488 particles in the ocean (DeLong et al., 1993). A broad range of species associated with γ -Pro was known to
489 be important for quorum sensing processes due to their high population density (Doberva et al., 2015)
490 associated with sinking or suspended aggregates (Krupke et al., 2016). In particular, the genus of γ -Pro such
491 as *Alteromonas* and *Pseudomonas*, are well-known quorum-sensing bacteria that can rely on diverse
492 signaling molecules to affect particle-associated bacterial communities by coordinating gene expression
493 within the bacterial populations (Long et al., 2003; Fletcher et al., 2007).

494 It has been reported that the growths of some bacterial strains of the γ -Pro such as *Alteromonas* spp.
495 and *Pseudomonas* spp. could be stimulated and regulated by oxylipins like PUAs (Ribalet et al., 2008; Pepi
496 et al., 2017). Oxylipins were found to promote biofilm formation of *Pseudomonas* spp. (Martinez et al.,
497 2016) and could serve as signaling molecules mediating cell-to-cell communication of *Pseudomonas* spp.
498 by an oxylipin-dependent quorum sensing system (Martinez et al., 2019). As PUAs are an important group
499 of chemical cues belonging to oxylipins (Franzè et al., 2018), it is thus reasonable to expect that PUAs may
500 also participate as potential signaling molecules for the quorum sensing among a high-density *Alteromonas*
501 or *Pseudomonas*. A high level of particle-adsorbed PUAs occurring on organic particles in the low-oxygen
502 water would likely allow particle specialists such as *Alteromonas* to regulate bacterial community structure,
503 which could alter species richness and diversity of PAB as well as their metabolic functions such as
504 respiration and production when interacting with particulate organic matter in the hypoxic zone. Various
505 bacterial assemblages may have different rates and efficiencies of particulate organic matter degradation
506 (Ebrahimi et al., 2019). Coordination amongst these PAB could be critical in their ability to thrive on the
507 recycling of POC (Krupke et al., 2016) and thus likely contribute to the acceleration of oxygen utilizations

508 in the hypoxic zone. Nevertheless, the molecular mechanism of the potential PUA-dependent quorum
509 sensing of PAB may be an important topic for future study.

510 Our findings may likely apply to other coastal systems where there are large river inputs, intense
511 phytoplankton blooms driven by eutrophication, and strong hypoxia, such as the Chesapeake Bay, the
512 Adriatic Sea, and the Baltic Sea. For example, Chesapeake Bay is largely influenced by river runoff with
513 strong eutrophication-driven hypoxia during the summer as a result of increased water stratification (Fennel
514 and Testa, 2019) and enhanced microbial respiration fueled by organic carbons produced during spring
515 diatom blooms (Harding et al., 2015). Similar to the PRE, there was also a high abundance of γ -Pro in the
516 low-oxygen waters of the Chesapeake Bay associated with the respiration of resuspended organic carbon
517 (Crump et al., 2007). Eutrophication causes intense phytoplankton blooms in the coastal ocean.
518 Sedimentation of the phytoplankton carbons will lead to their accumulation in the surficial sediment
519 (Cloern, 2001), including PUFA compounds derived from the lipid production. Resuspension and oxidation
520 of these PUFA-rich organic particles during summer salt-wedge intrusion might lead to high
521 particle-adsorbed PUAs in the water column. These PUAs could likely shift the particle-attached bacterial
522 community to consume more oxygen when degrading particulate organic matter and thus potentially
523 contribute to the formation of seasonal hypoxia. In this sense, the possible role of PUAs on coastal hypoxia
524 may be a byproduct of eutrophication driven by anthropogenic nutrient loading. Further studies are required
525 to quantify the contributions from PUAs-mediated oxygen loss by aerobic respiration to total
526 deoxygenation in the coastal ocean.

527

528 **5. Conclusions**

529 In summary, we found elevated concentrations of pPUAs and dPUAs in the hypoxic waters below the
530 salt-wedge. We also found high particle-adsorbed PUAs associated with particles of $>25\ \mu\text{m}$ in the hypoxic
531 waters based on the large-volume filtration method, which could generate a hotspot PUAs concentration
532 of $>10\ \mu\text{mol L}^{-1}$ in the water column. In the hypoxic waters, bacterial respiration was largely controlled by

533 PAB (>0.8 μm) with FLB (0.2-0.8 μm) only accounting for 25-30% of the total respiration. Field
534 PUA-amended experiments were conducted for PAB associated with particles of >25 μm retrieved from the
535 low-oxygen waters. We found distinct responses of PAB (>25 μm) to different doses of PUAs treatments
536 with an increase of cell growth in response to low-dose PUAs (1 $\mu\text{mol L}^{-1}$) but an elevated cell-specific
537 metabolic activity including bacterial respiration and production in response to high-dose PUAs (100 μmol
538 L^{-1}). Improved cell-specific metabolism of PAB in response to high-dose PUAs was also accompanied by a
539 substantial shift of bacterial community structure with increased dominance of genus *Alteromonas* within
540 the γ -Pro.

541 Based on these observations, we hypothesize that PUAs may potentially act as signaling molecules for
542 coordination among the high-density PAB below the salt-wedge, which would likely allow bacteria such as
543 *Alteromonas* to thrive in degrading particulate organic matters. Very possibly, this process by changing
544 community compositions and metabolic rates of PAB would lead to an increase of microbial oxygen
545 utilization that might eventually contribute to the formation of coastal hypoxia.

546
547 *Data availability.* Some of the data used in the present study are available in the Supplement. Other data
548 analyzed in this article are tabulated herein. For any additional data please request from the corresponding
549 author.

550
551 *Supplement.* The supplement related to this article is available online at: [bg-2020-243-supplement](#).

552
553 *Author Contributions.* Q.P.L designed the project. Z.W. performed the experiments. Q.P.L and Z.W. wrote
554 the paper with inputs from all co-authors. All authors have given approval to the final version of the
555 manuscript.

556
557 *Competing interests.* The authors declare no competing financial interest.

558

559 *Acknowledgements.* We are grateful to the captains and the staff of *R/V Haike68* and *R/V Tan Kah Kee* for
560 help during the cruises. We thank Profs Dongxiao Wang (SCSIO) and Xin Liu (XMU) for organizing the
561 cruises, Mr. Yuchen Zhang (XMU) for field assistances, Profs Changsheng Zhang (SCSIO) and Weimin
562 Zhang (GIM) for analytical assistance, as well as Prof. Dennis Hansell (RSMAS) for critical comments.

563

564 *Financial support.* This work was supported by the National Natural Science Foundation of China
565 (41706181, 41676108), the National Key Research and Development Program of China
566 (2016YFA0601203), and the Key Special Project for Introduced Talents Team of Southern Marine Science
567 and Engineering Guangdong Laboratory (Guangzhou) (GML2019ZD0305). ZW also wants to
568 acknowledge a visiting fellowship (MELRS1936) from the State of Key Laboratory of Marine
569 Environmental Science (Xiamen University).

570 **REFERENCE**

- 571 Balestra, C., Alonso-Saez, L., Gasol, J. M., and Casotti, R.: Group-specific effects on coastal bacterioplankton of
572 polyunsaturated aldehydes produced by diatoms, *Aquat. Microb. Ecol.*, 63, 123-131,
573 <http://doi.org/10.3354/ame01486>, 2011.
- 574 Bartual, A., Morillo-Garcia, S., Ortega, M. J., and Cozar, A.: First report on vertical distribution of dissolved
575 polyunsaturated aldehydes in marine coastal waters, *Mar. Chem.*, 204, 1-10.
576 <https://doi.org/10.1016/j.marchem.2018.05.004>, 2018.
- 577 Breitburg, D., Levin, L. A., Oschlies, A., Gregoire, M., Chavez, F. P., Conley, D. J., Garcon, V., Gilbert, D., Gutierrez,
578 D., Isensee, K., Jacinto, G. S., Limburg, K. E., Montes, I., Naqvi, S. W. A., Pitcher, G. C., Rabalais, N. N.,
579 Roman, M. R., Rose, K. A., Seibel, B. A., Telszewski, M., Yasuhara, M., and Zhang, J.: Declining oxygen in the
580 global ocean and coastal waters, *Science*, 359, eaam7240, <http://doi.org/10.1126/science.aam7240>, 2018.
- 581 Cloern, J. E.: Our evolving conceptual model of the coastal eutrophication problem, *Mar. Ecol. Prog. Ser.*, 210:
582 223-253, <http://doi.org/10.3354/meps210223>, 2001.
- 583 Crump, B. C., Peranteau, C., Beckingham, B., and Cornwell J. C.: Respiratory succession and community succession
584 of bacterioplankton in seasonally anoxic estuarine waters, *Appl. Environ. Microb.*, 73, 6802-6810,
585 <http://doi.org/10.1128/aem.00648-07>, 2007.
- 586 Crump, B. C., Baross, J. A., and Simenstad, C. A.: Dominance of particle-attached bacteria in the Columbia River
587 estuary, USA. *Aquat. Microb. Ecol.*, 14, 7-18, <http://doi.org/10.3354/ame014007>, 1998.
- 588 Delong, E. F., Franks, D. G., and Alldredge, A. L.: Phylogenetic diversity of aggregate-attached vs free-living marine
589 bacterial assemblages, *Limnol. Oceanogr.* 38: 924-934, <http://doi.org/10.4319/lo.1993.38.5.0924>, 1993.
- 590 Diaz, R. J., and Rosenberg, R.: Spreading dead zones and consequences for marine ecosystems, *Science*, 321,
591 926-929, <http://doi.org/10.1126/science.1156401>, 2008.
- 592 Doberva, M., Sanchez-Ferandin, S., Toulza, E., Lebaron P., and Lami, R.: Diversity of quorum sensing autoinducer
593 synthases in the Global Ocean Sampling metagenomic database, *Aquat. Microb. Ecol.* 74: 107-119,
594 <http://doi.org/10.3354/ame01734>, 2015.
- 595 Doney, S. C., Ruckelshaus, M., Duffy, J. E., Barry, J. P., Chan, F., English, C. A., Galindo, H. M., Grebmeier, J. M.,
596 Hollowed, A. B., Knowlton, N., Polovina, J., Rabalais, N. N., Sydeman, W. J., and Talley, L. D.: Climate change
597 impacts on marine ecosystems, *Annu. Rev. Mar. Sci.*, 4, 11-37,
598 <http://doi.org/10.1146/annurev-marine-041911-111611>, 2012.
- 599 Dyksterhouse, S. E., Gray J. P., Herwig R. P., Lara J. C. and Staley J. T.: *Cycloclasticus pugetii* gen. nov., sp. nov., an
600 aromatic hydrocarbon-degrading bacterium from marine sediments, *Int. J. of Syst. Bacteriol.*, 45: 116-123,
601 <http://doi.org/10.1099/00207713-45-1-116>, 1995.
- 602 Edwards, B. R., Bidle, K. D., and van Mooy, B. A. S.: Dose-dependent regulation of microbial activity on sinking
603 particles by polyunsaturated aldehydes: implications for the carbon cycle, *P. Natl. Acad. Sci. USA.*, 112,
604 5909-5914, <http://doi.org/10.1073/pnas.1422664112>, 2015.
- 605 Ebrahimi, A., Schwartzman, J., and Cordero, O. X.: Cooperation and self-organization determine rate and efficiency

606 of particulate organic matter degradation in marine bacteria, *P. Natl. Acad. Sci. USA.*, 116, 23309-23316,
607 <http://doi.org/10.1073/pnas.1908512116>, 2019.

608 Fennel, K., and Testa, J. M.: Biogeochemical Controls on Coastal Hypoxia, *Annu. Rev. Mar. Sci.*, 11, 4.1-4.26,
609 <http://doi.org/10.1146/annurev-marine-010318-095138>, 2019.

610 Fletcher, M. P., Diggle, S. P., Crusz, S. A., Chhabra, S. R., Camara, M., and Williams, P.: A dual biosensor for
611 2-alkyl-4-quinolone quorum-sensing signal molecules, *Environ. Microbiol.*, 9: 2683-2693,
612 <http://doi.org/10.1111/j.1462-2920.2007.01380.x>, 2007.

613 Franzè, G., Pierson, J. J., Stoecker, D. K., and Lavrentyev, P. J.: Diatom-produced allelochemicals trigger trophic
614 cascades in the planktonic food web, *Limnol. Oceanogr.*, 63, 1093-1108, <http://doi.org/10.1002/lno.10756>, 2018.

615 Galeron, M. A., Radakovitch, O., Charriere, B., Vaultier, F., Volkman, J. K., Bianchi, T. S., Ward, N. D., Medeiros, P.
616 M., Sawakuchi, H. O., Tank, S., Kerherve, P., and Rontani, J. F.: Lipoxygenase-induced autoxidative degradation
617 of terrestrial particulate organic matter in estuaries: A widespread process enhanced at high and low latitude, *Org.*
618 *Geochem.*, 115, 78-92, <http://doi.org/10.1016/j.orggeochem.2017.10.013>, 2018.

619 García-Martín, E. E., Aranguren-Gassis, M., Karl, D. M., et al.: Validation of the in vivo Iodo-Nitro-Tetrazolium
620 (INT) salt reduction method as a proxy for plankton respiration. *Front. Mar. Sci.*, 6, 220,
621 <http://doi.org/10.3389/fmars.2019.00220>, 2019

622 Garneau, M.E., Vincent, W.F., Terrado, R., and Lovejoy, C.: Importance of particle-associated bacterial heterotrophy
623 in a coastal Arctic ecosystem, *J. Marine Syst.*, 75, 185-197, <http://doi.org/10.1016/j.jmarsys.2008.09.002>, 2009.

624 Ge, Z., Wu, Z., Liu Z., Zhou, W., Dong, Y., and Li, Q. P.: Using detaching method to determine the abundance of
625 particle-attached bacteria from the Pearl River Estuary and its coupling relationship with environmental factors,
626 *Chinese J. Mar. Environ. Sci.*, <http://doi.org/10.12111/j.mes.20190065>, 2020.

627 Harding, Jr. L. W., , Adolf, J. E., Mallonee, M. E., Miller, W. D., Gallegos, C. L., Perry, E. S., Johnson, J. M., Sellner,
628 K. G., and Paerl H. W.: Climate effects on phytoplankton floral composition in Chesapeake Bay, *Estuar. Coast.*
629 *Shelf S.*, 162, 53-68, <http://doi.org/10.1016/j.jecss.2014.12.030>, 2015.

630 He, B. Dai, M., Zhai, W., Guo, X., and Wang, L.: Hypoxia in the upper reaches of the Pearl River Estuary and its
631 maintenance mechanisms: A synthesis based on multiple year observations during 2000-2008, *Mar. Chem.*, 167,
632 13-24, <http://doi.org/10.1016/j.marchem.2014.07.003>, 2014.

633 Hopkinson, C.S.: Shallow-water benthic and pelagic metabolism- evidence of heterotrophy in the nearshore Georgia
634 bight, *Mar. Biol.*, 87, 19-32, <http://doi.org/10.1007/bf00397002>, 1985.

635 Helm, K. P., Bindoff, N. L., and Church, J. A.: Observed decreases in oxygen content of the global ocean, *Geophys.*
636 *Res. Lett.*, 38, L23602. <http://doi.org/10.1029/2011GL049513>, 2011.

637 Hmelo, L. R., Mincer, T. J., and Van Mooy, B. A. S.: Possible influence of bacterial quorum sensing on the hydrolysis
638 of sinking particulate organic carbon in marine environments, *Env. Microbiol. Rep.*, 3, 682-688,
639 <http://doi.org/10.1111/j.1758-2229.2011.00281.x>, 2011.

640 Huang, Y., Liu, X., Laws, E. A., Chen, B., Li, Y., Xie, Y., Wu, Y., Gao, K., and Huang, B.: Effects of increasing
641 atmospheric CO₂ on the marine phytoplankton and bacterial metabolism during a bloom: A coastal mesocosm

642 study, *Sci. Total Environ.*, 633, 618-629, <http://doi.org/10.1016/j.scitotenv.2018.03.222>, 2018.

643 Hu, J., Zhang H., and Peng P.: Fatty acid composition of surface sediments in the subtropical Pearl River estuary and
644 adjacent shelf, Southern China. *Estuar. Coast, Shelf S.*, 66: 346-356, <http://doi.org/10.1016/j.ecss.2005.09.009>,
645 2006.

646 Ianora, A., and Miralto, A.: Toxigenic effects of diatoms on grazers, phytoplankton and other microbes: a review,
647 *Ecotoxicology*, 19, 493-511, <http://doi.org/10.1007/s10646-009-0434-y>, 2010.

648 Ivars-Martinez, E., Martin-Cuadrado, A. B., D'Auria, G., Mira, A., Ferriera, S., Johnson, J., et al.: Comparative
649 genomics of two ecotypes of the marine planktonic copiotroph *Alteromonas macleodii* suggests alternative
650 lifestyles associated with different kinds of particulate organic matter. *ISME*, J2, 1194–1212, 2008.

651 Kemp, W. M., Testa, J. M., Conley, D. J., Gilbert, D., and Hagy, J. D.: Temporal responses of coastal hypoxia to
652 nutrient loading and physical controls, *Biogeosciences*, 6, 2985-3008, <http://doi.org/10.5194/bg-6-2985-2009>,
653 2009.

654 Krupke, A., Hmelo, L. R., Ossolinski, J. E., Mincer, T. J., and Van Mooy, B. A. S.: Quorum sensing plays a complex
655 role in regulating the enzyme hydrolysis activity of microbes associated with sinking particles in the ocean,
656 *Front. Mar. Sci.*, 3:55, <http://doi.org/10.3389/fmars.2016.00055>, 2016.

657 Kirchman D. L.: Leucine incorporation as a measure of biomass production by heterotrophic bacteria, in: *Hand book*
658 *of methods in aquatic microbial ecology*, edited by: Kemp, P. F., Cole, J. J., Sherr, B. F., and Sherr, E. B., Lewis
659 Publishers, Boca Raton, 509–512, <http://doi.org/10.1201/9780203752746-59>, 1993.

660 Kirchman D. L.: *Microbial ecology of the oceans*, 2nd Ed., Hoboken, New Jersey, Wiley, 1-593,
661 <http://doi.org/10.1002/9780470281840>, 2008.

662 Lee, S., Lee, C., Bong, C., Narayanan, K., and Sim, E.: The dynamics of attached and free-living bacterial population
663 in tropical coastal waters, *Mar. Freshwater Res.*, 66, 701-710, <http://doi.org/10.1071/mf14123>, 2015.

664 Long, R. A., Qureshi, A., Faulkner, D. J., and Azam, F.: 2-n-pentyl-4-quinolinol produced by a marine *Alteromonas*
665 sp and its potential ecological and biogeochemical roles, *Appl. Environ. Microb.*, 69, 568-576,
666 <http://doi.org/10.1128/aem.69.1.568-576.2003>, 2003.

667 Lu, Z., Gan, J., Dai, M., Liu, H., and Zhao, X.: Joint effects of extrinsic biophysical fluxes and intrinsic
668 hydrodynamics on the formation of hypoxia west off the Pearl River Estuary, *J. Geophys. Res.-Oceans.*, 123,
669 <https://doi.org/10.1029/2018JC014199>, 2018.

670 Lunau, M., Lemke, A., Walther, K., Martens-Habbena, W., and Simon, M.: An improved method for counting
671 bacteria from sediments and turbid environments by epifluorescence microscopy, *Environ. Microbiol.*, 7,
672 961-968, <http://doi.org/10.1111/j.1462-2920.2005.00767.x>, 2005.

673 Marie, D., Partensky, F., Jacquet, S. and Vaulot, D.: Enumeration and cell cycle analysis of natural populations of
674 marine picoplankton by flow cytometry using the nucleic acid stain SYBR Green I, *Appl. Environ. Microbiol.*,
675 63, 186-193, <http://doi.org/10.1128/AEM.63.1.186-193.1997>, 1997.

676 Martinez, E., and Campos-Gomez, J.: Oxylipins produced by *Pseudomonas aeruginosa* promote biofilm formation
677 and virulence, *Nat. Commun.*, 7, 13823, <https://doi.org/10.1038/ncomms13823>, 2016.

678 Martinez, E., Cosnahan, R. K., Wu, M. S., Gadila, S. K., Quick, E. B., Mobley, J. A., and Campos-Gomez, J.:
679 Oxylipins mediate cell-to-cell communication in *Pseudomonas aeruginosa*, *Commun. Biol.*, 2, 66,
680 <https://doi.org/10.1038/s42003-019-0310-0>, 2019.

681 Oudot, C., Gerard, R., Morin, P., and Gningue, I.: Precise shipboard determination of dissolved-oxygen (winkler
682 procedure) for productivity studies with a commercial system, *Limnol. Oceanogr.*, 33, 146-150,
683 <http://doi.org/10.4319/lo.1988.33.1.0146>, 1988.

684 Parsons, T. R., Maita, Y., and Lalli, C. M.: Fluorometric Determination of Chlorophylls, in: *A manual of chemical*
685 *and biological methods for seawater analysis*, Pergamum Press, Oxford, 107-109,
686 <http://doi.org/10.1016/B978-0-08-030287-4.50034-7>, 1984.

687 Paul, C., Reunamo, A., Lindehoff, E., et al.: Diatom derived polyunsaturated aldehydes do not structure the
688 planktonic microbial community in a mesocosm study, *Mar. Drugs*, 10, 775-792,
689 <http://doi.org/10.3390/md10040775>, 2012.

690 Pepi, M., Heipieper, H. J., Balestra, C., Borra, M., Biffali, E., and Casotti, R.: Toxicity of diatom polyunsaturated
691 aldehydes to marine bacterial isolates reveals their mode of action, *Chemosphere*, 177, 258-265, 2017

692 Pohnert, G.: Wound-activated chemical defense in unicellular planktonic algae, *Ange. Chem. Int. Edit.*, 39, 4352-4354.
693 [https://doi.org/10.1002/1521-3773\(20001201\)39:23<4352::AID-ANIE4352>3.0.CO;2-U](https://doi.org/10.1002/1521-3773(20001201)39:23<4352::AID-ANIE4352>3.0.CO;2-U), 2000

694 Rabouille, C., Conley, D. J., Dai, M. H., Cai, W. J., Chen, C. T. A., Lansard, B., Green, R., Yin, K., Harrison, P. J.,
695 Dagg, M., and McKee, B.: Comparison of hypoxia among four river-dominated ocean margins: The Changjiang
696 (Yangtze), Mississippi, Pearl, and Rhone rivers, *Cont. Shelf Res.*, 28, 1527-1537,
697 <http://doi.org/10.1016/j.csr.2008.01.020>, 2008.

698 Ribalet, F., Intertaglia, L., Lebaron, P., and Casotti, R.: Differential effect of three polyunsaturated aldehydes on
699 marine bacterial isolates, *Aquat. Toxicol.*, 86, 249-255, <http://doi.org/10.1016/j.aquatox.2007.11.005>, 2008.

700 Robinson, C., and Williams, P. J. I.: Respiration and its measurement in surface marine waters, in: *Respiration in*
701 *Aquatic Ecosystems*, edited by de Giorgio, P. A., and Williams, P. J. I., Oxford University Press, New York,
702 147-180, <http://doi.org/10.1093/acprof:oso/9780198527084.003.0009>, 2005.

703 Su, J., Dai, M., He, B., Wang, L., Gan, J., Guo, X., Zhao, H., and Yu, F.: Tracing the origin of the oxygen-consuming
704 organic matter in the hypoxic zone in a large eutrophic estuary: the lower reach of the Pearl River Estuary, China,
705 *Biogeosciences*, 14, 4085-4099, <http://doi.org/10.5194/bg-14-4085-2017>, 2017.

706 Vidoudez, C., Casotti, R., Bastianini, M., and Pohnert, G.: Quantification of dissolved and particulate polyunsaturated
707 aldehydes in the Adriatic Sea. *Mar. Drugs*, 9, 500-513, <https://doi.org/10.3390/md9040500>, 2011.

708 Wang, N., Lin, W., Chen, B., and Huang, B.: Metabolic states of the Taiwan Strait and the northern South China Sea
709 in summer 2012, *J. Trop. Oceanogr.*, 33, 61-68, <http://doi.org/doi:10.3969/j.issn.1009-5470.2014.04.008>, 2014.

710 Williams, P. J. I. and de Giorgio, P. A.: Respiration in Aquatic Ecosystems: history and background, in: *Respiration in*
711 *Aquatic Ecosystems*, edited by de Giorgio, P. A., and Williams, P. J. I., Oxford University Press, New York, 1-17,
712 <http://doi.org/10.1093/acprof:oso/9780198527084.003.0001>, 2005.

713 Wu, Z., and Li, Q. P.: Spatial distributions of polyunsaturated aldehydes and their biogeochemical implications in the

714 Pearl River Estuary and the adjacent northern South China Sea, *Prog. Oceanogr.*, 147, 1-9,
715 <http://doi.org/10.1016/j.pocean.2016.07.010>, 2016.

716 Xu, J., Li, X., Shi, Z., Li, R., and Li, Q. P.: Bacterial carbon cycling in the river plume in the northern South China
717 Sea during summer, *J. Geophys. Res.-Oceans*, 123, 8106-8121, <http://doi.org/10.1029/2018jc014277>, 2018.

718 Yin, K., Lin, Z., and Ke, Z.: Temporal and spatial distribution of dissolved oxygen in the Pearl River Estuary and
719 adjacent coastal waters, *Cont. Shelf Res.*, 24, 1935-1948, <http://doi.org/10.1016/j.csr.2004.06.017>, 2004.

720 Zhang, H., and Li, S.: Effects of physical and biochemical processes on the dissolved oxygen budget for the Pearl
721 River Estuary during summer, *J. Marine Syst.*, 79, 65-88, <http://doi.org/10.1016/j.jmarsys.2009.07.002>, 2010.

722 Zhang, Y., Xiao, W., and Jiao, N.: Linking biochemical properties of particles to particle-attached and free-living
723 bacterial community structure along the particle density gradient from freshwater to open ocean, *J. Geophys.*
724 *Res.-Biogeo.*, 121, 2261-2274, <http://doi.org/10.1002/2016jg003390>, 2016.

725 **Table 1.** Summary of treatments in the experiments of exogenous PUAs additions for the low-oxygen
726 waters at station Y1 during June 2019. The PUAs solution includes heptadienal (C7_PUA), octadienal
727 (C8_PUA), and decadienal (C10_PUA) with the mole ratios of 10:1:10.
728

		Treatment
1	Control (methanol)	methanol
2	Low-dose PUAs (methanol)	2 mM PUAs in methanol
3	High-dose PUAs (methanol)	200 mM PUAs in methanol

729
730

Figures and Legends

Figure 1: Sampling map of the Pearl River Estuary and the adjacent northern South China Sea during (A) June 17th-28th, 2016, (B) June 18st-June 2nd, 2019. Contour shows the bottom oxygen distribution with white lines highlighting the levels of 93.5 $\mu\text{mol kg}^{-1}$ (oxygen-deficient zone) and 62.5 $\mu\text{mol kg}^{-1}$ (hypoxic zone); dashed line in panel A is an estuary-to-shelf transect with blue dots for three stations with bacterial metabolic rate measurements; diamonds in panel B are two stations with vertical pPUAs and dPUAs measurements with Y1 the station for PUAs-amended experiments.

Figure 2: Procedure of large-volume filtration and subsequent experiments. A large volume of the low-oxygen water was filtered through a 25- μm filter to obtain the particles-adsorbed PUAs and the particle-attached bacteria (PAB). The carbon-source test of PUA for the inoculated PAB includes the additions of PUA, alkanes (ALK), and polycyclic aromatic hydrocarbons (PAH). PUAs-amended experiments for PAB include Control (CT), Low-dose (PL), and High-dose PUAs (PH). Samples in the biological oxygen demand (BOD) bottles at the end of the experiment were analysed for bacterial respiration (BR), abundances (BA), production (BP) as well as DNA. Note that pPUAs and dPUAs are particulate and dissolved PUAs in the seawater.

Figure 3: Vertical distributions of (A) temperature, (B) turbidity, (C) nitrate, (D) salinity, (E) dissolved oxygen, and (F) chlorophyll-*a* from the estuary to the shelf of the NSCS during June 2016. Section locations are shown in Figure 1; the white line in panel D shows the area of oxygen deficiency zone ($<93.5 \mu\text{mol kg}^{-1}$).

Figure 4: Comparisons of oxygen, bulk bacterial respiration (BR) and production (BP), as well as bulk bacterial abundances (BA) of α -Proteobacteria (α -Pro), γ -Proteobacteria (γ -Pro), Bacteroidetes (Bact), and other bacteria for the bottom waters between stations inside (X1) and outside (X2 and X3) the hypoxic zone during the 2016 cruise. Bulk bacteria community includes FLB and PAB of $<20 \mu\text{m}$. Locations of stations X1, X2, X3 are showed in Figure 1A. Error bars are the standard deviations.

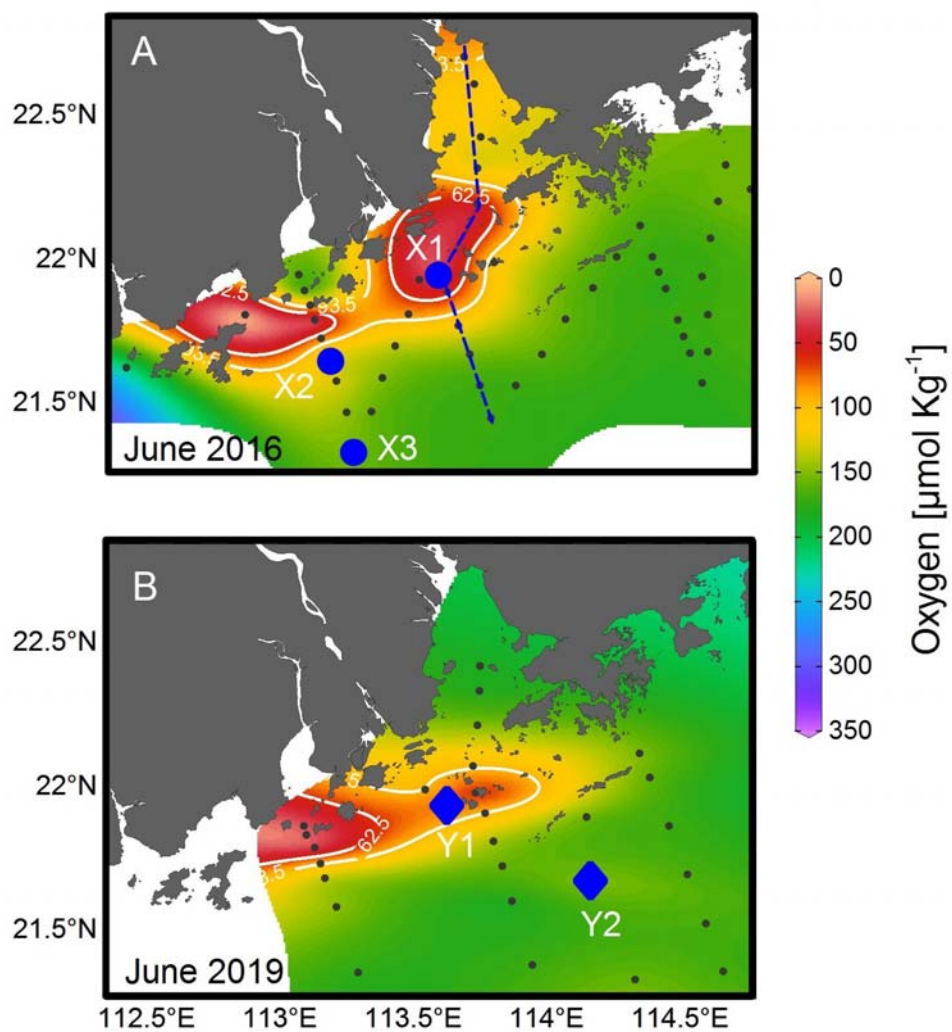
Figure 5: Vertical distributions of (A) temperature, (B) salinity, (C) dissolved oxygen (DO), (D) chlorophyll-*a* (Chl-*a*), (E) particulate PUAs (pPUAs) and (F) dissolved PUAs (dPUAs) inside (Y1) and outside (Y2) the hypoxic zone during June 2019. Locations of station Y1 and Y2 are shown in Figure 1. Error bars are the standard deviations.

764 **Figure 6:** Concentrations of particle-adsorbed PUAs (in micromoles per liter particle) in the middle (12 m)
765 and the bottom (25 m) waters of station Y1 during June 2019. Three different PUA components are also
766 shown including heptadienal (C7_PUA), octadienal (C8_PUA), and decadienal (C10_PUA). Error bars are
767 the standard deviations.

768
769 **Figure 7:** Responses of particle-attached bacterial parameters including (A) bacterial abundance (BA_{particle}),
770 (B) bacterial respiration (BR_{particle}), (C) cell-specific bacterial respiration (sBR_{particle}), (D) bacterial growth
771 efficiency (BGE_{particle}), (E) bacterial production (BP_{particle}), and (F) cell-specific bacterial production
772 (sBP_{particle}) to different doses of PUAs additions at the end of the experiments for the middle (12 m) and the
773 bottom waters (25 m) at station Y1. Error bars are standard deviations. The star represents a significant
774 difference ($p < 0.05$) with PL and PH the low and high dose PUA treatments and C the control.

775
776 **Figure 8:** Variation of particle-attached bacterial community compositions on (A) the phylum level and (B)
777 the genus level in response to different doses of PUAs additions at the end of the experiments for the
778 middle and the bottom waters at station Y1. Labels PL and PH are for the low- and high-dose PUAs with
779 CT the control.

780
781 **Figure 9:** Carbon-source test of PUAs with cell culture of particle-attached bacteria inoculated from the
782 low-oxygen waters of station Y1 including the initial conditions (Day0) at the beginning of the experiments
783 as well as results after 30 days of incubations (Day30) for (A, B) the middle and (C, D) the bottom waters,
784 respectively. Bottles from left to right are the mediums (M) with the additions of polycyclic aromatic
785 hydrocarbons (M+PAH, 200 ppm), alkanes (M+ALK, 0.25 g L^{-1}), and heptadienal (M+C7_PUA, 0.2 mmol
786 L^{-1}); Note that a change of turbidity should indicate bacterial utilization of organic carbons. (E) the optical
787 density of bacterium *Alteromonas hispanica* MOLA151 growing in the minimal medium as well as in the
788 mediums with the additions of mannitol, pyruvate, and proline (M+MPP, 1% each), heptadienal
789 (M+C7_PUA, $145 \mu\text{M}$), octadienal (M+C8_PUA, $130 \mu\text{M}$), and decadienal (M+C10_PUA, $106 \mu\text{M}$). The
790 method for *A. hispanica* growth and the data in panel E are from Ribalet et al., 2008.



792

793

794

795

Figure 1

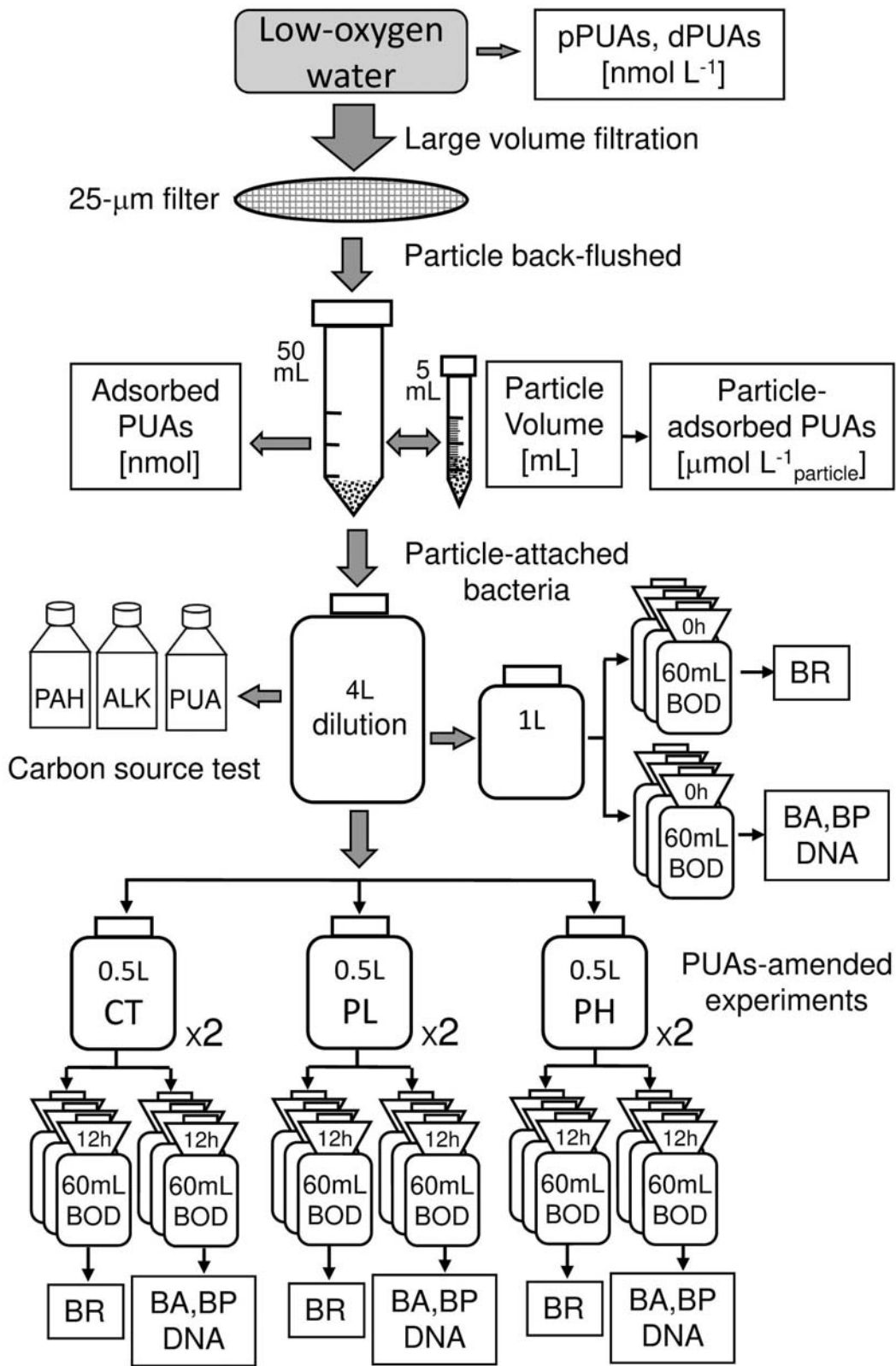


Figure 2

796

797

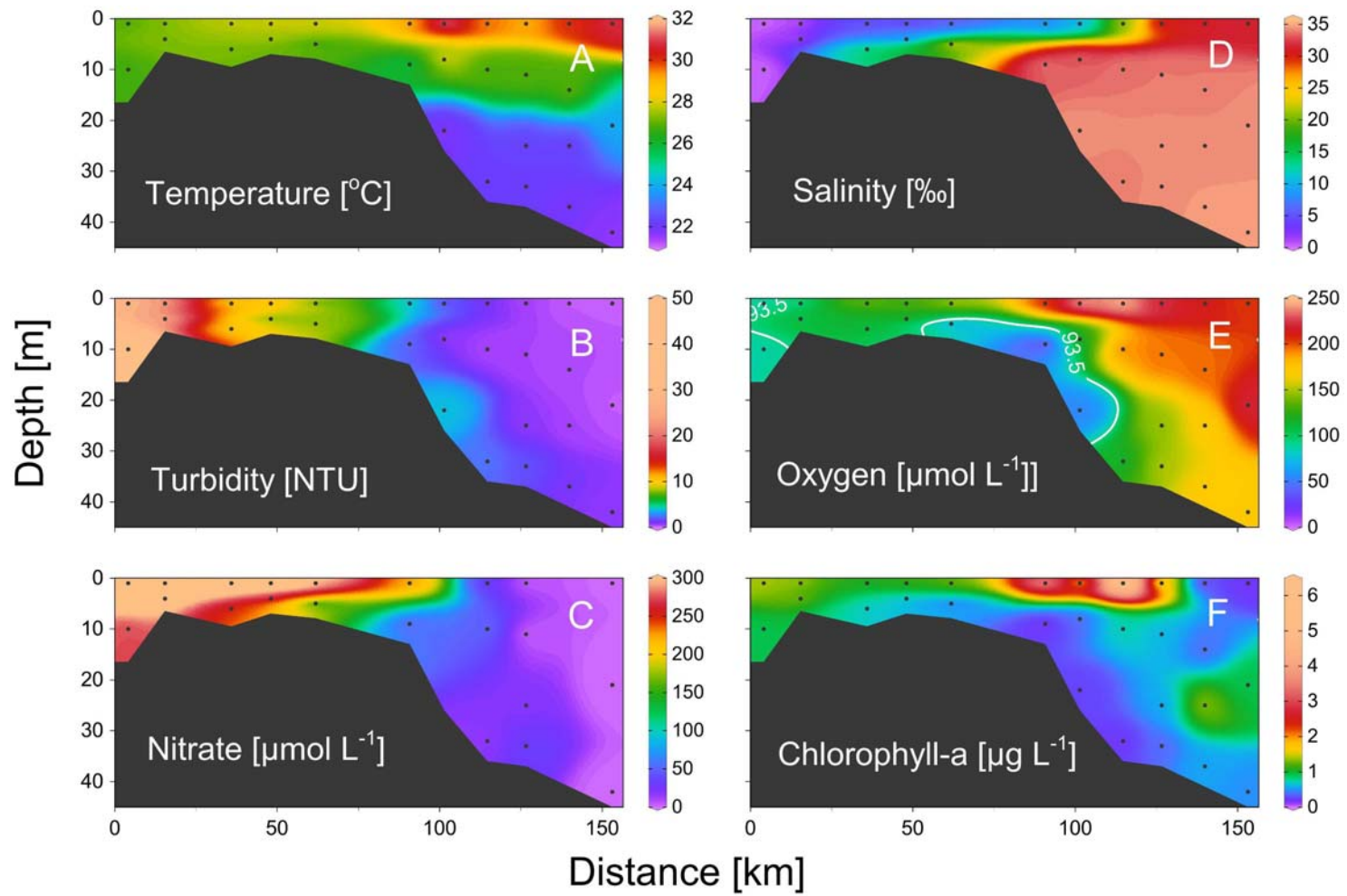
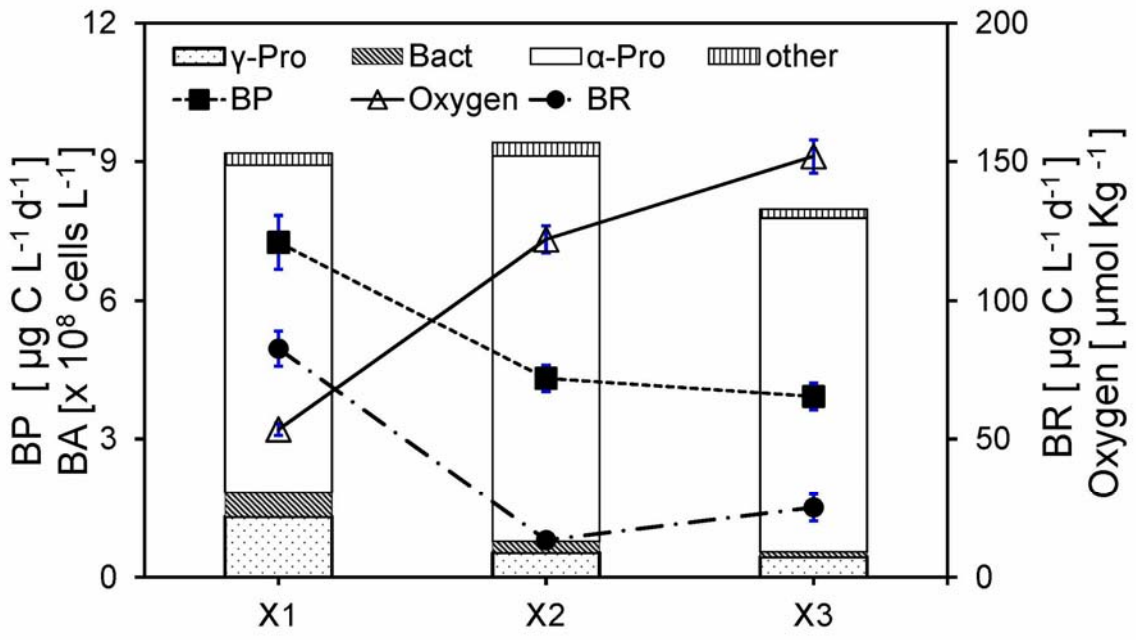


Figure 3

798
799
800



801
802
803
804

Figure 4

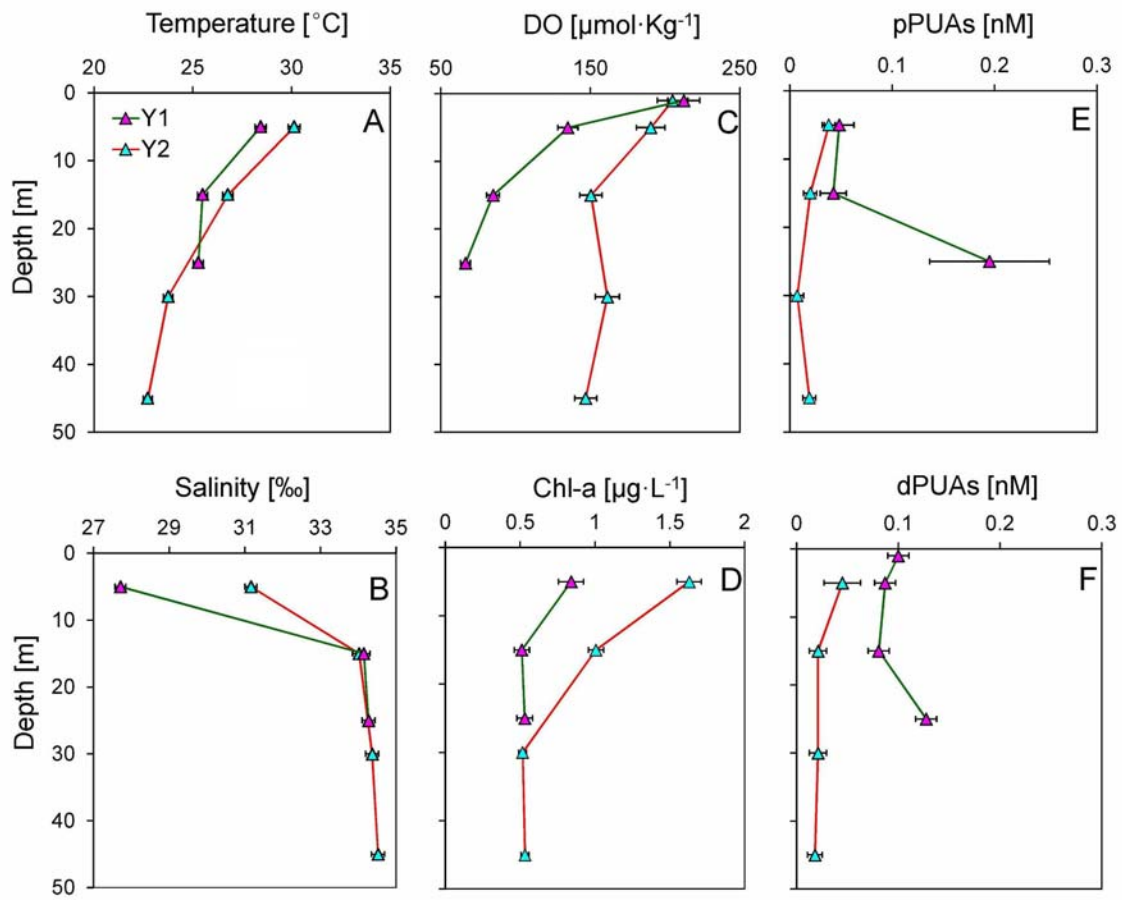


Figure 5

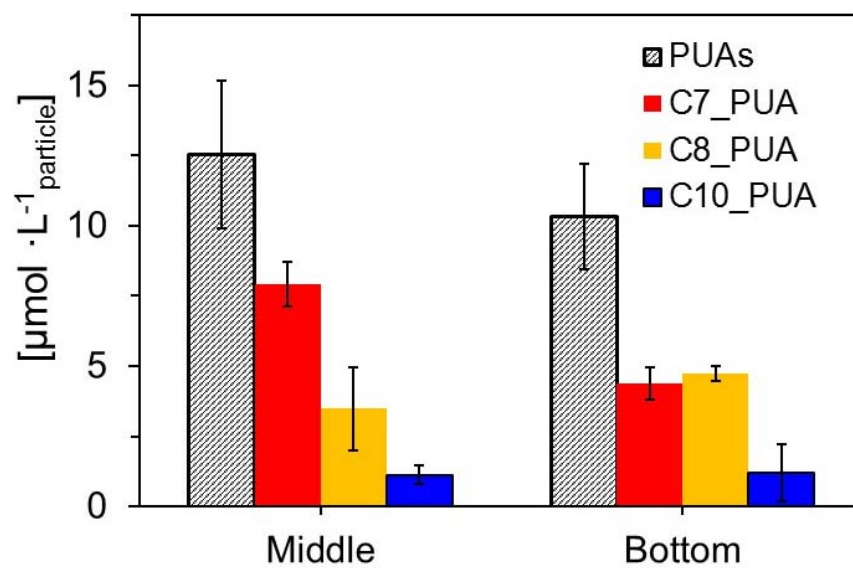
805

806

807

808

Particle adsorbed PUAs



809
810
811
812

Figure 6

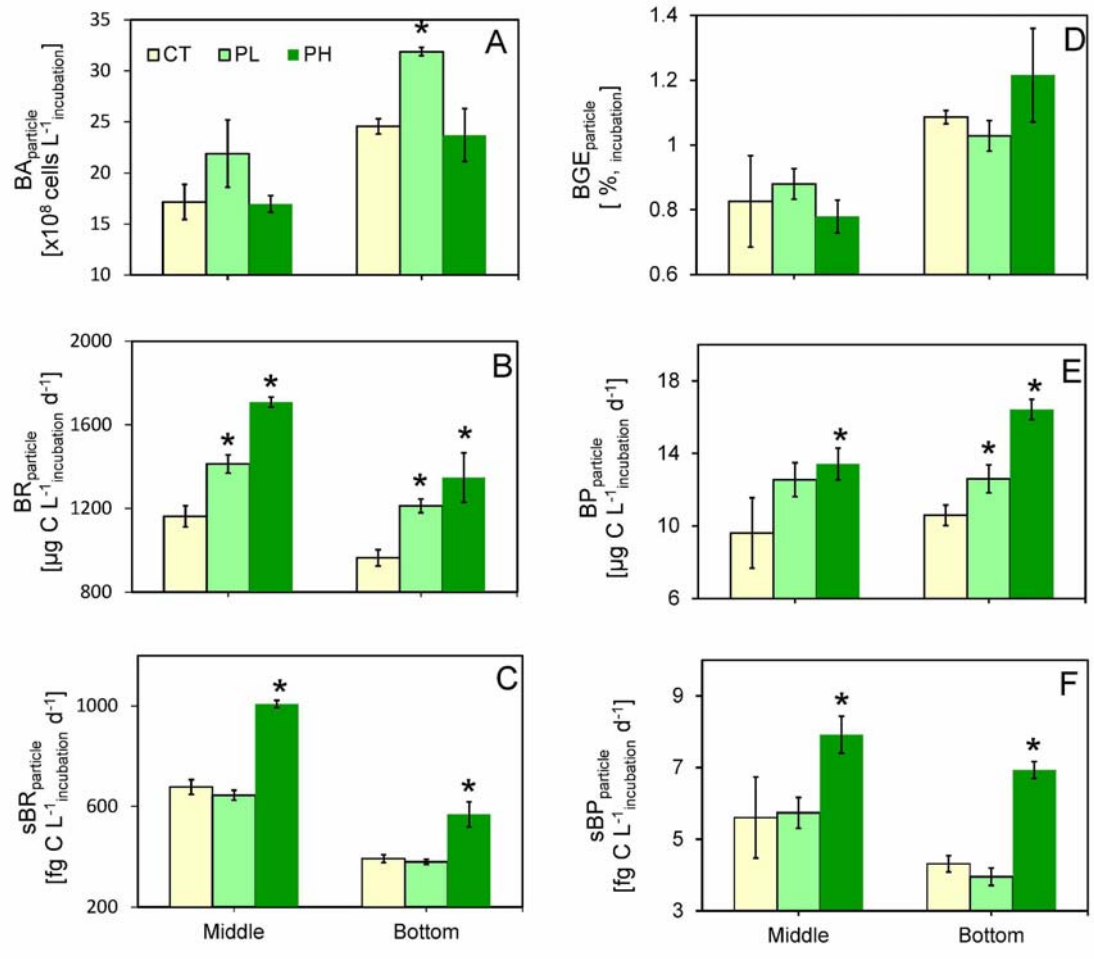


Figure 7

813
814
815
816

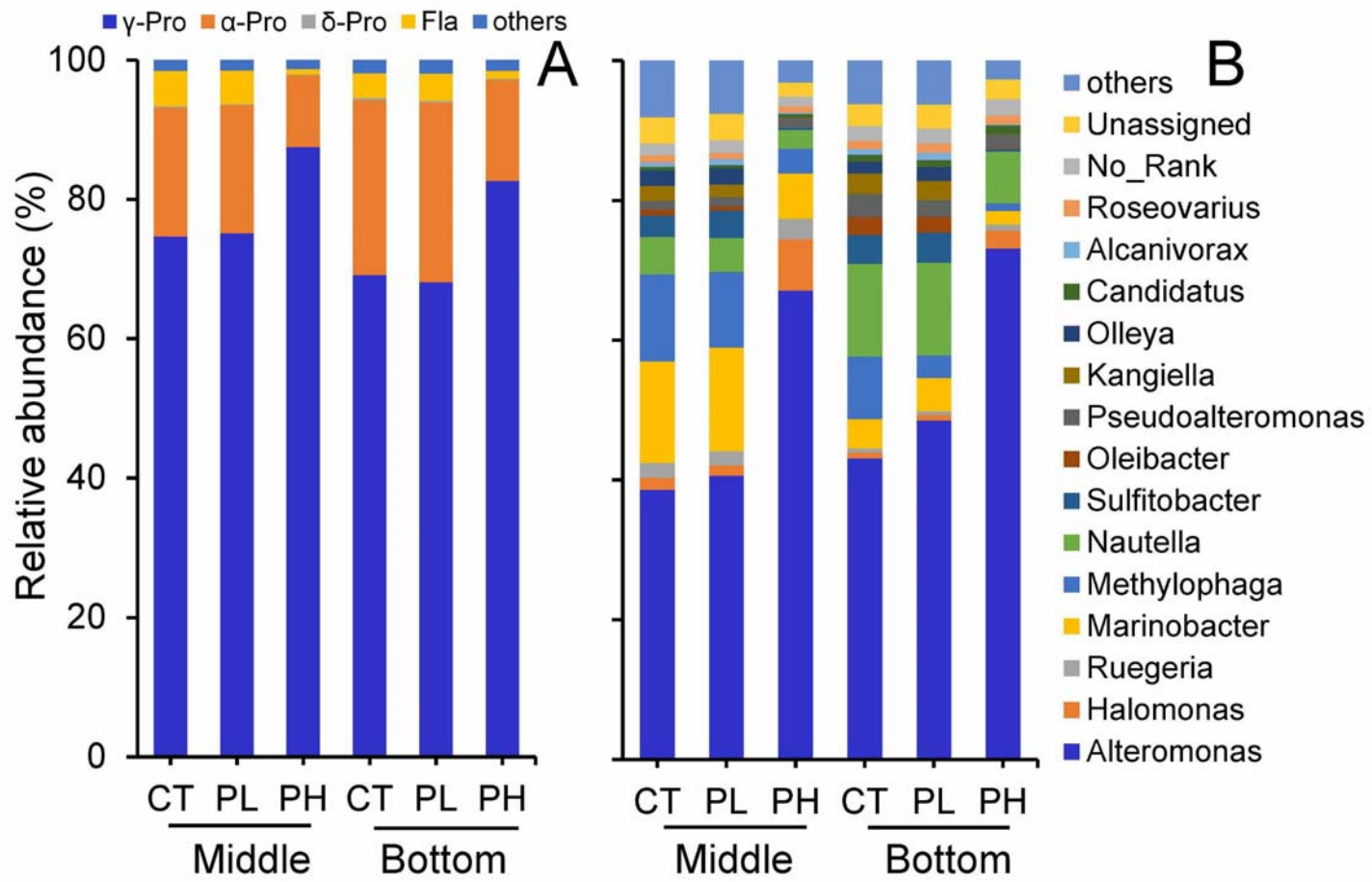
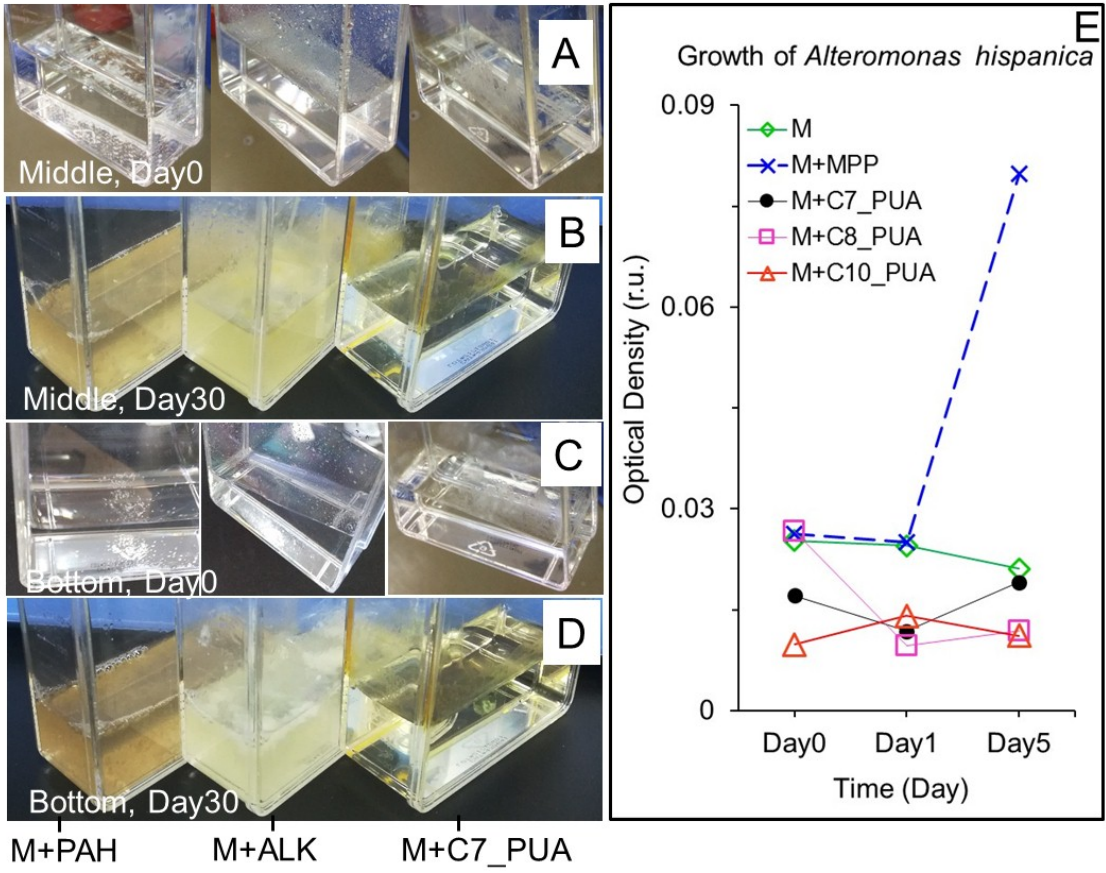


Figure 8

817

818

819



820
821
822
823

Figure 9